INTERNATIONAL ATOMIC ENERGY AGENCY
UNITED NATIONS EDUCATIONAL, SCIENTIFIC AND CULTURAL ORGANIZATION

INTERNATIONAL CENTRE FOR THEORETICAL PHYSICS
34100 TRIESTE (ITALY) - P.O.B. 586 - MIRAMARE - STRADA COSTIERA 11 - TELEPHONES: 224281/2/3/4/5/6
CABLE: CENTRATOM - TELEX 460392-I

SMR/113 - 1

AUTUMN COLLEGE

ON

THE TROPOSPHERE, STRATOSPHERE AND MESOSPHERE

10 September - 19 October 1984

THE MST RADAR TECHNIQUE

J. RÖTTGER

EISCAT Scientific Association
Box 705
S-981 27 Kiruna
Sweden

no. 1

Review Paper for MAP Handbook on Ground Based Techniques for Measuring Middle Atmosphere Parameters
January 1984

The MST Radar Technique

Jürgen Röttger[1]
EISCAT Scientific Association
Kiruna, Sweden

Abstract: This tutorial review gives a general overview on the coherent radar technique with special emphasis to mesosphere-stratosphere-troposphere (MST) radars operating in the VHF band. Some basic introduction to Doppler radar measurements and the radar equation is followed by an outline of the characteristics of atmospheric turbulence, viewed from the scattering and reflection processes of radar signals. MST radar signal acquisition and preprocessing, namely coherent detection, digital sampling, pre-integration and coding, is briefly discussed. The data analysis is represented in terms of the correlation and spectrum analysis, yielding the essential parameters: power, signal-to-noise ratio, average and fluctuating velocity and persistency. The techniques to measure wind velocities, viz. the different modes of the Doppler method as well as the spaced antenna method are surveyed and the feasibilities of the MST radar interferometer technique are elucidated. A general view on the criteria to design phased array antennas, used in most MST radar systems, is given. An outline of the hardware of a typical MST radar system is presented, which consists of the transmitter-receiver part, the radar controller and the data acquisition unit. In conclusion, some typical results are depicted, presently planned and operational radars are surveyed and a brief outlook for future requirements for MST radar systems is attempted.

1. Introduction

The origin of MST radars dates back to the early days of ionospheric backscatter observations which were carried out with a 41 MHz radar in Illinois/USA by Bowles (1958). Strong echoes, observed at 75-90 km height, were interpreted as due to "ionospheric scattering of the turbulence variety" in the mesosphere. Subsequently, Flock and Balsley (1967) reported about VHF radar observations at Jicamarca/Peru, which confirmed echoes from 75 km height and were also interpreted to be most likely caused by turbulence scattering in the presence of a gradient of electron density. Several years later Ronald F. Woodman with Alberto Guillén (1974) substantially improved the technique in order to measure velocities and they also reported the detection of stratospheric returns. They recognized the great potential of this technique for remote sounding of the middle atmosphere. Their studies triggered the evolution of a new generation of radars for atmospheric research, and VHF radars were started thereafter to be developed for the only purpose of lower and middle atmosphere observations.
Although earlier expectations that the entire region of the mesosphere, stratosphere and troposphere, which gave the name "MST" radar, could be monitored more or less continuously, have emerged to be an overestimate, their very unique applications to investigate the structure and dynamics of the middle atmosphere is widely accepted (Gage and Balsley, 1978; Walker, 1979; Balsley and Gage, 1980; Crane, 1980; Harper and Gordon, 1980; James, 1980; Röttger, 1980a; Klostermeyer, 1981; Rastogi, 1981; Woodman, 1981; Larsen and Röttger, 1982; Larsen, 1983a). It has turned out that the MST radar technique is also very suitable for operational applications in meteorology (Lhermitte, 1979; Wilson et al., 1980; Röttger, 1981a; Balsley and Gage, 1982; Hogg et al., 1983; Larsen 1983b). It is, thus, expected that further useful information on atmospheric physics will be obtained from continued MST radar observations, and these will also gain substantial contributions for the Middle Atmosphere Program.

MST radars make use of scattering and reflection from variations of humidity, temperature and electron density, induced by turbulence in the lower and middle atmosphere. Essentially, MST radars can observe: the 3-dimensional wind field, atmospheric reflectivity and stability, and morphology of turbulence and waves. The continuous measurements with MST radars offer very good quality and quantity middle atmosphere observations of wind velocities (Gage and Van Zandt, 1981). MST radars operate at frequencies around 50 MHz, and therefore are also called VHF radars (VHF = very high frequency band between 30 MHz and 300 MHz). Higher frequency radars mostly cover only the troposphere and stratosphere. Typical peak powers of VHF radars are between 1 kW and 1 MW. Range resolutions down to about 100 m and time resolutions down to some ten seconds are possible. The antenna arrays with typical dimensions of 1000 m^2 to some 10 000 m^2 point close to the zenith direction. Coherent detection, digital

---

[1] on leave from Max-Planck-Institut für Aeronomie, W.Germany

control and data acquisition are mandatory. We notice that the instrumental technique as well as the data acquisition and analysis are now basically developed, elaborated and fairly mature.

This tutorial review aims to give a general summary and overview on the state of art achieved during the first decade of the MST radar technique. It is intended to yield also a brief introduction to the atmospheric radar technique with special emphasis to MST radar applications. It is not intended to represent a review for experts working in this field, but rather to give an overview to outsiders as well as to allow a basic introduction for those who are planning to join this research field. For more specific technical descriptions of the atmospheric radar technique, the reader is referred to other books and articles, such as those by Skolnik (1970), Hardy (1972), Wilson and Miller (1972), Battan (1973), Gossard and Strauch (1983). Very detailed descriptions of MST radar techniques can be found in another Handbook for MAP (Bowhill, 1984).

In this paper a short introduction to the radar technique with special emphasis to MST radars is given in section 2, followed by an outline of characteristics of atmospheric turbulence which gives rise to the MST echoes (section 3). In sections 4 and 5 the data acquisition and digital preprocessing as well as some fundamentals of data analyses are discussed. In section 6 techniques to measure velocities are treated and some essentials of the interferometer technique, recently appplied to MST radars, are elucidated. Fundamentals of antenna designs are sketched in section 7 and a brief overview on the transmitter-receiver system and the radar control is presented in section 8. In section 9, empirical estimates of MST radar sensitivity, supported by a few typical results, are discussed. Finally, in section10 a list of planned and operational MST radars as well as a short outline of expected future developments is added.

2. Introduction to MST Radar Principles

2.1 Pulse operation

Let a pulsed electromagnetic wave be transmitted at the time T_1 (see Fig.1). The pulse duration of this radar signal shall be Δt_t.For simplification the pulse shape is assumed to be rectangular, but in real applications it may be a smoothed trapezoid or triangle or Gaussian shaped. In a non-dispersive propagation medium the pulse travels with the speed of light C and reaches the range r_a after the time $t_1=r_a/C$. A target at r_a can scatter or reflect the radar signal in some directions. A small fraction returns to the location of the transmitter, where this radar echo will be received after the time $t_1' = 2t_1 = 2r_a/C$. This yields the basic relation $r=C\cdot t/2$, which allows determination of the range of any radar target by measuring the roundtrip time t. This relation holds for monostatic radars (transmitter and receiver are at almost the same location). For bistatic radars (receiver separated from transmitter by a distance comparable to or larger than the ranges to the target) a modified expression has to be applied. Bistatic or multistatic operation will not be discussed here, since it is not too suitable for most MST radar applications.

Since the transmitted pulse has a finite duration Δt_t, its trailing edge will reach the range r_a at a time $t_1+\Delta t_t$, and reach the receiver at $2t_1+\Delta t_t$. If the radar target is a thin reflecting surface (called discrete, single or hard target), the shape of the received pulse is the replica of the transmitted pulse. Now assume that many scatterers fill all ranges along the radar beam. It is then obvious from Fig.1 that echoes from the range between $r_a - \Delta r/2$ and r_a reach the receiver simultaneously at t_1', and those from r_a to $r_a+\Delta r/2$ are received at $t_1'+\Delta t_t$. The pulse of duration Δt_t, thus, at one time illuminates a volume at r_a extended along a range $\Delta r=C\cdot\Delta t_t/2$. This is the range gate or range cell from which the radar echoes are received. Fig.1 shows that most of the echo power results from the range r_a, and minimum power is received from $r_a\pm\Delta r/2$. Thus, the resulting range weighting function of the single range gate centered around r_a is a triangle.

Because of the finite receiver bandwidth (usually matched to the bandwidth of the transmitted pulse) the receiver gate has a finite width in time. The receiver pulse response (given by about the inverse of the receiver bandwidth) distorts the received pulse by smoothing its leading and trailing edges and thus delaying it by about the receiver response time. The transmitter pulse length Δt_t, to which the receiver response time is matched, determines the range resolution Δr. The instrumental distortions of the radar pulse are not depicted in Fig.1 to maintain the clearness of survey, but they eventually have to be considered in the final analysis of the radar data.

In radar applications short pulses are normally transmitted periodically, i.e. the n-th pulse follows the (n-1)-th pulse after a specified time. For convenience it is set here to be a multiple (K>1) of Δt_t. This time (T_n-T_{n-1}) is called the interpulse period T_{IPP}. Its inverse is called the pulse repetition frequency $f_{PRF}=1/T_{IPP}$. The off-on-ratio of the transmitter $T_{IPP}/\Delta t_t-1$ determines approximately the range from which radar echoes can be unambiguously received (in units of range resolution). It is more customary, however, to use the ratio $d=\Delta t_t/T_{IPP}$, which is called duty cycle or duty factor. The transmitted power P_a, to be averaged over (more than) one interpulse period, is the product of the duty cycle and the transmitted pulse peak power P_p, i.e. $P_a=d\cdot P_p$.

Because in normal radar operations the pulse repetition frequency is kept constant, i.e. the transmitted pulse train is periodic, range-aliasing may occur. This ambiguity is depicted in Fig.1. At time t_2' an echo of pulse T_2 is received from range r_a, and an echo of pulse T_1 is received from range r_b. Of course higher order range-aliasing can occur from ranges $r_n=C\cdot(t+(n-1)\cdot T_{IPP})/2$. Because these echoes return from separate scatter volumes, the echo signals are uncorrelated but still their power accumulates in the same receiver range gate. If no special arrangements (e.g. pulse-coding or non-periodic T_{IPP}) are being made, the maximum unambiguous range is $r_{max} = C\cdot T_{IPP}/2$. The minimum range r_{min} obviously is given by the pulse duration Δt_t plus some instrumentally entailed transition time between transmission and reception.

2.2 Doppler measurements

Assume that a bulk motion carries the scatterers or reflectors in the volume at range r. Because of the Doppler effect, the rate of change of phase ϕ of the returned signal is then $d\phi/dt=4\pi/\lambda_o \cdot dr/dt$, where λ_o is the radar wavelength. When V' is the (radial) velocity in direction of the radar signal path, $V'=dr/dt$. The phase change $d\phi/dt$ is the angular Doppler frequency $\omega_D = 2\pi f_D$, which yields $f_D=-2V'/\lambda_o$. Since the radar signal is pulsed at a frequency f_{PRF}, i.e. the radar echo is sampled at a rate T_{IPP}, this yields the maximum Doppler frequency to be resolved by pulse-to-pulse analysis (Nyquist frequency): $f_{Dmax} = f_{PRF}/2 = 1/2T_{IPP}$. If coherent preintegration over 2N interpulse periods is applied, the effective sampling time is increased to $2N \cdot T_{IPP}$ (section 4.3), and f_{Dmax} has to be replaced by $f_N = 1/4NT_{IPP}$. This corresponds to a maximum radial velocity $V'_{max} = \lambda_o \cdot f_{Dmax}/2$ and $V'_{max} = \lambda_o \cdot C/8r_{max}$. It turns out for MST radars that V'_{max}, as defined here, is much larger than any realistic velocity. We will readily recognize this as well as deduce some obvious experimental advantages by estimating some typical numbers for the above defined radar parameters.

MST radars operate in the lower VHF band around 50 MHz, corresponding to wavelengths around 6 m. Since quasi-vertical antenna beam directions are used, ranges are roughly equal to altitudes. For MST radar observations of the middle atmosphere the range limits r_{max} are between 10 km and 100 km. This yields typical pulse repetition frequencies between 10 kHz and 1 kHz. Altitude resolutions from about 1 km down to at least 100 m are required to resolve typical vertical scales in the middle atmosphere. This corresponds to pulse lengths of about 1-10 µs. Thus, typical duty cycles are between about 10^{-1} and 10^{-3}.

Knowing that radial velocities with quasi-vertical radar beams do not exceed several 10 ms^{-1}, the Doppler frequency will barely exceed 10 Hz. Applying $f_{PRF} > 1$ kHz, the radar echo will be heavily oversampled, i.e. its phase and amplitude does vary little from pulse to pulse. This is called a coherent radar echo, in contrast to an incoherent radar echo which randomly changes phase and amplitude from one pulse to the next. One does make efficient use of the characteristic coherency of MST radar echoes to improve the data acquisition procedures (section 4.3). The differences between coherent radars, used to study the lower and middle atmosphere, and incoherent (scatter) radars, used to study the ionosphere with the Thomsom scatter technique, will be described in a different paper (Röttger, 1984).

2.3 Radar equation for scattering and reflection

Assume that the radar echo power is due to volume scatter and the scatterers totally fill the radar beam. Then the mean received radar echo power P_s is given by the radar equation:

$$P_s = \frac{A \cdot P_a \cdot \eta \cdot \Delta r}{4\pi r^2} , \qquad (1a)$$

where A is the effective antenna area (see section 7.1) and η is the radar reflectivity (see section 3.2).

If the radar echo is due to reflection from a hard target, e.g. a large surface stratified perpendicular to the radar wave propagation, the received radar echo power P_r is given by:

$$P_r = \frac{P_a \cdot A^2 \cdot |\varrho|^2}{\lambda_o^2 \cdot r^2} , \qquad (1b)$$

where ϱ is the amplitude reflection coefficient of the surface.

As compared to radar echoes from single hard targets (e.g. airplanes), where the echo power is proportional to r^{-4}, P_s and P_r are proportional to r^{-2}. This is simply explained by the fact that the volume or the region illuminated by the radar beam, are not constant but increase with the square of the range. However, restricting assumptions have to be fulfilled here: The most essential are that the illuminated volume has to be totally filled with scatterers and a reflecting surface has to be larger than the first Fresnel zone ($D=\sqrt{r\lambda_o}$). If more than one reflecting surface is in the radar volume, $|\varrho|^2$ has to be replaced by $R^2=\Delta r \cdot (F\bar{M})^2$, where F is a calibration constant and $\bar{M}$ is the mean generalized refractive index gradient (e.g., Hocking and Röttger, 1983).

If one assumes that the mechanisms of reflection and scattering are independent of each other, the total received echo power is

$$\bar{P} = P_r + P_s = P_a \cdot A \cdot \Delta r \cdot (C_r^2 + C_s^2) \cdot r^{-2} \qquad (2)$$

with the contribution due to reflection $C_r^2 = A \cdot (F\bar{M})^2/\lambda_o^2$,
and the contribution due to scattering $C_s^2 = \eta/4\pi$.
Both, C_r^2 and C_s^2, are dependent on properties of the reflecting and scattering media, evaluated at scales of half the radar wavelength λ_o and C_r^2 is additionally weighted by the instrumental parameters, antenna area A and the wavelength λ_o.

The theoretical treatments of these processes are based on the same formalism, namely the Born approximation, i.e. the amplitude of the scattered spherical wave is negligible compared to the amplitude of the incident plane wave. The three-dimensional statistical approach is based either on isotropic or on anisotropic volume scatter. The one-dimensional approach, treated in a statistical manner, describes Fresnel scatter which leads to similar results as for anisotropic volume scatter. The one-dimensional deterministic approach describes the reflection process.

Following early observations with MST radars operating in the lower VHF-band, it is now accepted that scattering and reflection contribute to the radar echoes (Gage and Green, 1978; Röttger and Liu, 1978; Gage and Balsley, 1980; Röttger, 1980b), but fairly often the limits between these two processes are not readily determinable in an experiment. It was therefore proposed to use the term effective reflectivity $c^2=c_r^2+c_s^2$. Depending on whether c_r^2 or c_s^2 is dominating the signal (see Röttger, 1980b, and Rastogi and Röttger, 1982, for more detailed discussions), the basic processes are either called reflection or scattering.

Different terms are used to specify these processes, namely specular, partial or Fresnel reflection if a single reflecting surface dominantly contributes to the radar echo, and Fresnel scatter if several statistically independent surfaces in the radar range gate produce the echoes. If it is found that the reflecting surfaces are rough and corrugated, then the term diffuse reflection is used. Also isotropic volume scatter is observed.

3. Atmospheric Turbulence Causing VHF Radar Echoes

3.1. Characteristics of turbulence spectra

The basic condition for any kind of scatter and reflection is the existence of spatial variations of the refractive index at scales of half the radar wavelength. These variations can be caused by atmospheric waves or by turbulence. The turbulence can be active (just generated) or fossil (remnants of active turbulence), and it is partly generated by waves. It is often a question of how to distinguish turbulence from waves, but one still can describe the energy cascade of atmospheric waves and turbulence by means of their spatial and temporal spectra. These items are not discussed here and more information can be found elsewhere, e.g. Gage (1979), Klostermeyer (1981), Woodman (1981), Larsen (1983a), VanZandt and Vincent (1983).

The spatial spectrum of atmospheric turbulence is basically characterized by three subranges. In the buoyancy subrange, variations are controlled by buoyancy forces and the scales of the anisotropic eddies are typically larger than a scale L_o which is some ten to hundred meters in the middle atmosphere. Since these scales are larger than the wavelengths of VHF radars, they do not contribute to the scattering/reflection process. There is a transfer of energy from eddies in the buoyancy subrange through the inertial subrange to smaller eddies. The subrange transition is at L_o, which is also called the outer scale of the inertial subrange or the Kolmogorov macroscale. Turbulence at scales of several meters in the inertial subrange yields the VHF radar echoes. At the inner scale l_o (also called Kolmogorov microscale) another transition takes place into the viscous subrange. The turbulence, decaying down to scales in this range, is heavily damped by viscosity, and refractive index variations at scales smaller than l_o are so small that they do not contribute to detectable radar signal scattering.

The Kolmogorov microscale l_o changes strongly as a function of altitude, because it is inversely proportional to the density. It also depends on temperature and turbulence intensity which causes uncertainties about its mean value by many 10%. The mean l_o is less than some centimeters in the lower troposphere. It exponentially increases with height to several centimeters near the tropopause, to about a meter near the stratopause and to about ten meters near the mesopause. VHF-radars with Bragg wavelengths λ_B (half the operating wavelength λ_o for backscatter) of about 3m are therefore able to detect echoes from altitudes up to near the mesopause. Depending on the scattering/reflection mechanism, they could observe the entire altitude region of the mesosphere, stratosphere and troposphere, which led to the introduction of the name of MST radars. In contrast, radars operating in the upper VHF band ($\lambda_B \approx 1$ m) and in the UHF band (λ_B=5-50 cm) can detect echoes from turbulence only up to at most the middle stratosphere. Therefore, these are called ST radars. We do not include the incoherent or Thomson scatter radars in this nomenclature, which detect echoes from free electrons in the ionosphere, and thus can cover the altitude range of the mesosphere and the thermosphere (see Mathews, this handbook volume).

3.2 Turbulence refractive index structure constant

The reflected and scattered echo power is given by the component of the spatial spectrum of the variation of the refractive index n (also called refractivity here), whose wavelength is one half the radar wavelength. The reflected echo power depends on the shape n(r) of the refractive index discontinuity. In general, the steeper the gradient of the refractive index the larger the reflection coefficient; steps in the refractive index must not be much greater in spatial extent than a quarter wavelength, otherwise destructive interference occurs and will strongly reduce the reflection coefficient. It obviously follows that a longer-wavelength radar will see a larger reflection coefficient than a shorter-wavelength radar for a given profile of refractive index. Different models of refractive index profiles can yield the same reflection coefficient. This means that a deduction of refractive index variations from the reflected radar echo is generally ambiguous.

Let us assume that atmospheric turbulence mixes the refractive index profile and the associated gradients so that random irregularities of the refractive index result. The power which is scattered back then no longer results from reflection at a deterministic discontinuity, but from "reflection" at many disordered turbulent irregularities, which fill the volume defined by the pulse length and the antenna beam width (radar volume). Simply put, each irregularity has a single backscatter cross section. The total backscatter cross section per unit volume is the radar reflectivity η, which is related to the turbulent variations of the refractive index.

It is assumed that the turbulence is in the inertial subrange, which is given by the boundaries of the outer scale L_o, associated with macroscale turbulent eddies, and the inner scale l_o, where the turbulent irregularities start to be dissipated by

viscosity. In the inertial subrange the turbulence is assumed to be homogeneous and isotropic. Under these assumptions the radar reflectivity is $\eta = 0.39 \cdot C_n^2 \cdot \lambda_o^{-1/3}$. The quantity C_n^2 is called the turbulence refractive index structure constant. It is given by

$$C_n^2 \sim \overline{\Delta n^2} \cdot L_o^{-2/3},$$

and is a measure of the outer scale L_o of the inertial subrange of the turbulence spectrum and the mean square variations $\overline{\Delta n^2}$ of the refractive index n (e.g. Battan, 1973).

Since turbulence parameters determine the structure constant C_n^2, which in turn determines the radar reflectivity η and the scattered power P_s, it appears likely that information on turbulence can be deduced from the radar observations. Qualitative information (e.g. morphology of turbulence layers and their strength and persistency) is more definitely obtained than quantitative information (e.g. turbulence energy dissipation, diffusivity and viscosity, momentum transfer and wave breaking dynamics). The latter needs a very detailed treatment, since instrumental effects, separability of reflection and scattering, and further geophysical parameters (e.g. the mean gradient of refractive index) have to be considered. It is not in the scope of this paper to discuss these in detail. They, for instance, were treated by VanZandt et al. (1981), Hocking (1983a,b) and others. We only would like to outline those items which are most general to the application of the MST radar technique: 1) some basic information on turbulence is needed to estimate the sensitivity of radars: 2) echoes from refractivity variations are used as tracers to monitor the structure of the atmosphere and to measure bulk and fluctuating velocities.

The MST radar observations have shown that the turbulence at scales of some meters is often anisotropic. This causes some uncertainties in the deduction of turbulence parameters, but on the other hand gains a substantial increase of echo power, i.e. signal detectability due to reflection from the anisotropic irregularities. Strong evidence is found that isotropic and anisotropic turbulence irregularities coexist. A model which was earlier proposed by Bolgiano (1968) has recently found new interest and can explain some of the observations. In a turbulent layer vertical mixing tends to equalize mean gradients of the background refractive index. This consequently causes discontinuities at the top and the bottom of the layer. Since the turbulent layers have larger horizontal than vertical dimensions, these discontinuities of the refractive index have much larger horizontal than vertical dimensions, too. The discontinuities must often be as thin as several meters (in vertical extent) since they cause reflection of MST radar signals. They are also called stratifications, laminae or sheets. It is deduced from the observations that they are rough or corrugated because of the interaction with the turbulence layer. These sheets are often very persistent and it is assumed that they have a much longer lifetime than the originating turbulence layer,

which one may call "fossil turbulence". Another idea was recently brought forward by VanZandt and Vincent (1983) who proposed that the anisotropic reflectivity is due to low frequency buoyancy waves. Both models still require experimental verification.

1.3 Origin of refractivity changes

The refractive index variations discussed in the preceding paragraphs are directly related to variations of the atmospheric parameters: humidity, temperature, pressure (≙neutral density) and electron density. The mean refractive index in the lower and middle atmosphere is for VHF: $n = 1 + n_1' + n_2' + n_3'$, where $n_1' = 3.7 \cdot 10^{-1} \cdot e/T^2$, $n_2' = 77.6 \cdot 10^{-6} \cdot p/T$, and $n_3' = -40.3 \cdot N_e/f_o^2$,

with e = partial pressure of water vapor (humidity) in mb,

p = pressure in mb,

T = temperature in K,

N_e = number of free electrons per m^3,

f_o = radar operating frequency in Hz.

n_1' is called the wet term, n_2' the dry term, and n_3' the ionospheric term.

All three terms are very small compared to 1; their contribution to the refractive index yields only a few parts per thousand change. The variations of n, which cause the scattering and reflection, are evidently produced by turbulence induced variations of e, p, T and N_e. Although this is not too realistic, we assume for illustration that the average intensity of turbulence is constant with altitude. We then can estimate the relative contributions of e, p, T and N_e to the radar reflectivity, which is shown in Fig.2 (after Gage and Balsley, 1980). The wet term n_1' (humidity contribution) has to be considered only in the lowest few kilometers of the troposphere, whereas the dry term n_2' (temperature contribution) dominates up to the lower mesosphere. Contributions due to pressure fluctuations are normally negligible, but decreasing mean pressure with altitude has a strong influence on n_2'. For radars operating in the lower VHF band, the ionization of the D-region determines the refractive index in the height region between about 60 km and 90 km. Except of the ionospheric term n_3', the refractive index contributions are non-dispersive, i.e. frequency independent. Polarization and absorption effects can be neglected for VHF and UHF signals in the entire height range of the troposphere, stratosphere and mesosphere. At frequencies larger than about 50 MHz, the turbulence induced scatter term will get very weak in the mesosphere (because of the viscous subrange limitations) and the incoherent scatter term will dominate the signal. For scales in the inertial subrange, clear air turbulence in the mesosphere yields perturbations in the ionization (D-region irregularities) and it has to be stressed that these irregularities are not created by plasma instabilities. They are induced by turbulence in the neutral atmosphere because of the collisions between ionized and neutral molecules in this height region. The D-region irregularities are therefore replica of neutral air turbulence.

We could assume from Fig.2 that the entire altitude range up to 100 km could be monitored by VHF radars. However, apart from the inertial subrange limiting the VHF radar observations to altitudes below about 90 km (above this height occasionally only meteor echoes can be used), other limitations have to be considered. The refractivity contributions obviously change during varying atmospheric conditions. The electron density in the ionospheric D-region (60-90 km) is directly dependent on the solar zenith angle, and consequently the radar reflectivity of the mesosphere is relatively high only during the daylight hours. Solar flares can also generate short enhancements of the D-region ionization. At high latitudes additional ionization is often generated also during the night by particle precipitation effects during auroral disturbances. However, the strong dependence of the electron density with height very seldom yields sufficiently strong reflectivity for echoes to be deteced from heights below 60-65 km. Echoes from meteor induced ionization can be used to measure velocities in the altitude range 90-100 km (Avery et al., 1983). The stratospheric reflectivity is only determined by temperature variations, and this mostly holds also for the reflectivity in the upper troposphere. However, during convective processes water vapor may be carried up to the tropopause, which then yields a substantial increase of reflectivity (by n_1') in the upper troposphere. In the tropics the reflectivity may even be enhanced due to humidity contributions up to 15-18 km altitude.

The mean profile of reflectivity contributions shown in Fig.2 is not only varying because the averages n_1', n_2' and n_3' are varying, but is evidently modulated by the occurrence of turbulence and stable stratifications. Higher reflectivities for instance occur in regions which are most likely to be turbulent, e.g. jet streams in the upper troposphere and breaking of tides and gravity waves in the mesosphere, as well as in regions of enhanced static stability, e.g. the lower stratosphere.

As mentioned earlier, the radar signal strength depends on the product of the instrumental parameters, average power and antenna area (aperture), and the atmospheric parameter, effective reflectivity. The detectability of an echo is a function of the signal-to-noise ratio, and the noise level at VHF is given by the sky noise, which is constant when averaging over a day. The sensitivity or the minimum detectable reflectivity of MST radars therefore is directly proportional to the power-aperture product P·A. For illustration, typical low ($P \cdot A \approx 10^3$ Wm^2, e.g. early tests with the SOUSY-VHF-Radar (Röttger et al., 1978)) and high (Jicamarca VHF radar (Balsley, 1978a; Fukao et al.,1979)) power-aperture products are inserted in Fig.2 from which the observable height regions can approximately be estimated. These limits are for vertical antenna beams, i.e. they are essentially determined by reflection processes. The limits shift to the right for off-vertical beams when no reflection but only scattering is observed. These qualitative estimates should be used as guidelines only, and more quantitative estimates are discussed in section 9.

4. MST Radar Signal Acquisition and Preprocessing

The simplified schematics of an MST radar system, shown in Fig.3, are used for a basic explanation of the MST radar operation and data acquisition procedure. In an operational system many more components are used, but Fig.3 shows only those which are necessary for this explanation. For more details see Woodman and Guillén (1974), Röttger and Schmidt (1979), Schmidt et al., (1979), Carter et al. (1980), Clark and Carter (1980), Sato and Woodman (1980), Rastogi (1983), for instance.

4.1 Coherent detection

An oscillator generates a signal s^0 at the angular frequency $\omega_o=2\pi f_o$, where $f_o = C/\lambda_o$ is the centre radar operation frequency. A pulse train, generated by the radar controller, imposes a modulation to this signal. After amplification in the transmitter (TX) the radar signal

$$s(t)=a(t)\exp(i(\omega_o t+\varphi(t))) \qquad (3)$$

is transmitted, where a(t) determines an amplitude modulation (by the pulse train) and $\varphi(t)$ corresponds to a phase modulation (for coding), and $i=\sqrt{-1}$. a(t) and $\varphi(t)$ are slowly varying as compared to $\omega_o t$. The radar signal is scattered/reflected from the radar volume and reaches the receiver (RX) via the same or a separate antenna. Additionally, noise (sky noise and interference) is received and adds to the radar echo. The band-limited echo signal s' plus noise r can be represented by

$c'(t)=s'(t)+r(t) = a_1(t)\cos \omega_o t + i a_2(t)\sin \omega_o t,$

where a_1 and a_2 are independent Gaussian variables in a pure scattering process, and are correlated in a reflection process. The uncorrelated noise contributes only uncertainties to these estimates. After linear amplification in the receiver, $c'(t)$ is coherently detected by multiplicative mixing with s^0. After low-pass or post-detection filtering (to eliminate high frequency components $2\omega_o$, which are generated during mixing), this yields

$$c(t)= a^+(t)\cos \Psi^+(t) + i a^+(t)\sin \Psi^+(t),$$
$$\text{where } a^+(t)=(a_1^2(t) + a_2^2(t))^{1/2}/2, \qquad (4a)$$
$$\Psi^+(t)=\arctan (a_2(t)/a_1(t)).$$

The phase $\Psi^+(t)=\omega_D t-\Psi'(t)$ is given by the Doppler frequency $\omega_D=-4\pi V'/\lambda_o$, which is due to the bulk motion V' of the scatterers. The time variable phase $\Psi'(t)=\Psi(t)+\varphi(t)$, where $\Psi(t)$ is caused by the fluctuations of the scatterers/reflectors in the radar volume. The amplitude $a^+(t)$ is a measure of the reflectivity. These latter statements are only valid if the noise contributions are separated from the signal.

The coherently detected complex signal (+ noise) can be expressed in the form

$$c(t) = x(t) + iy(t), \qquad (4b)$$

where the real part $x(t)=a^+(t)\cos\Psi^+(t)$ is called the in-phase component, and the imaginary part $y(t)=a^+(t)\sin\Psi^+(t)$ is called the quadrature component. Both components, x and y, are called the quadrature components.

The Fourier transform of c(t) is $\tilde{A}(\omega)=\int c(t)\exp(-i\omega t)dt = \tilde{x}(\omega)+i\tilde{y}(\omega)$, which yields the power spectrum $P(\omega)= \tilde{x}^2 + \tilde{y}^2$. The measured $P(\omega)$ is the convolution of the spectrum of the refractivity fluctuations in the radar volume with the spectrum $P_T(\omega)$ of the transmitted wave form, multiplied by the bandpass characteristics $P_R(\omega)$ of the receiver. Since $P(\omega)$ is much narrower than the envelope of $P_T(\omega)$ and $P_R(\omega)$ in MST radar investigations, these instrumental effects can mostly be disregarded.

4.2 Digital sampling

In the analogue-digital converter (ADC) the signal c(t) is sampled at discrete time intervals $t_k=k\cdot\Delta t_s$. This is illustrated in Fig.4, which shows the amplitude variations of one of the quadrature components as they can be monitored with an oscilloscope connected to the output of the quadrature detector (after postdetection filtering). The sequences n=1,2,... can be assumed to represent successive oscilloscope beam deflections, triggered by the leading slope of the transmitter pulse. This pulse is strongly attenuated by receiver gating. It is flipped in phase φ by 180° from one pulse to the next (change from positive to negative amplitude), for reasons explained later. Corresponding to the transmitter-pulse phase φ, the sign of the signal also changes from one to the next interpulse period. For convenience the signal phase is shown here to be similar to the transmitter-pulse phase. The signal phase can take any values, however, depending on the length of the phase path from the transmitter to the radar volume.

On the vertical axis of Fig.4 the time t_k is given, which directly can be converted to range by means of the definitions of Fig.1. The sampling time interval Δt_s should be equal to the radar pulse length, since this yields an optimum matching to the range gate width or resolution Δr. The signal and the noise had passed the receiver and postdetection filters and are therefore bandlimited. The response time of the receiver, which is approximately inversely proportional to the filter bandwidth, should also be equal to Δt_s, respectively Δt_t. The subscript k of t_k is the serial number of the range gate with k=0,1,..., K-1, where k=0 corresponds to the beginning of the transmitter pulse. Since the quadrature components are digitally sampled, we can write (4b) in the form $c_k=x_k+iy_k$. We also call c_k the complex raw data samples.

The number of sampling time steps between successive radar transmitter pulses is K, which is also the number of sampled range gates. The interpulse period is $T_{ipp}= K\cdot\Delta t_s$. The cycle k=0,..., K-1 is repeated once with k'=0,..., K'-1 with a reversed phase of the transmitter pulse. Both cycles, denoted by k and k' (with $k' \hat{=} k$ and $K' \hat{=} K$), determine one radar cycle $2T_{IPP}$. The serial number of radar cycles is given by n=1,...,N. One radar burst is determined by N radar cycles, which last for $t_i=2N\cdot T_{IPP}$.

The generation of all pulse trains, needed to control these cycles of the transmitter and receiver-ADC-integrator system, is done in the radar controller (Fig.3). It is loaded by the host computer which is also used for further data processing.

Let us look at the time development of the signal + noise amplitude in the k-th range gate, which is sketched in Fig.5. In this example the digitally sampled quadrature components x_k and y_k consist of a quasi-harmonic oscillation (of period of about $50T_{IPP}$, regarded as signal) with superimposed random fluctuations (regarded as noise). The signal + noise is lifted by a bias up to the mean amplitude 1. The bias can be different for the x- and y-components but for convenience the bias is chosen here to be equal for both. The digital samples (dots and circles) are taken every second interpulse period (k). Samples of the intermediate interpulse period (k') lie between the depicted samples. They would show oscillations shifted by 180°, because of the transmitter phase flip from k to k'.

It is evident that the signal is oversampled, i.e. many more samples are taken than would be necessary to resolve the amplitude and phase of the harmonic oscillation. However, the noise is undersampled, since its time scale of fluctuation is much faster than the sampling rate given by T_{IPP}. The time scale of the noise fluctuations is proportional to the receiver response time ($\sim\Delta t_s$), and the time scale of the signal variations is given by the typical time scales τ_ξ and τ'_ξ of the scattering/reflection process. These latter times are inversely proportional to the Doppler frequency f_D and the average statistical phase changes $d\Psi/dt$. To give some typical numbers:

$\Delta t_s = 10^{-6}$s (for 150 m range resolution),

$T_{IPP} = 10^{-3}$s (f_{PRF} = 1 kHz),

$\tau'_\xi = 1/f_D > 10^{-1}$s ($f_D$ = 10 Hz),

$\tau_\xi = (d\Psi/dt)^{-1} \sim 10^{-1}$s (see section 5.2).

We will see later that τ_ξ and τ'_ξ can be more appropriately expressed by the autocorrelation function analysis. It is evident, that $\Delta t_s \ll T_{IPP} \ll \tau_\xi, \tau'_\xi$, which proves that the time scales of noise Δt_s are undersampled and the time scales of signal τ_ξ are oversampled.

The undersampling of noise, which has a bandwidth of the receiver postdetection filters, cannot be avoided because samples at a specified range gate cannot be taken more often than every interpulse period T_{IPP}. This undersampling means that all noise power (received within the receiver bandwidth) folds into the sampled spectrum which is limited by the Nyquist frequency $\pm 1/2T_{IPP}$. Since the noise samples are totally independent, because $\Delta t_s \ll T_{IPP}$, the undersampling does not cause problems. Because $\tau_\xi, \tau'_\xi \gg T_{IPP}$, the raw data signal samples are not independent, i.e. coherent.

4.3 Pre-integration and processing

The spectrum which one would obtain with the sampling rate T_{IPP} is very wide and mostly contains high frequency noise power. The signal power is confined to relatively low frequencies only ($f=1/\tau_\xi \ll 1/2T_{IPP}$). It is evident therefore that low pass filtering, done before the spectrum analysis, will not change the signal characteri-

stics but eliminates high frequency noise contributions. The simplest form of low pass filtering is just the complex addition of the signal + noise samples over an interval $t_i \ll \tau_\xi$. This is illustrated in Fig.5, where the larger circles indicate the averages over N=8 samples in each case of this example. A readily noticed effect of this averaging is the reduction of the number of total samples by a factor 1/N.

Since the noise (r) and the signal (s) are independent of each other, their quadrature components add to $c_{kn} = c^r_{kn} + c^s_{kn}$, where $c^r_{kn} = x^r_{kn} + iy^r_{kn}$ are the quadrature components of the noise and c^s_{kn} those of the signal. The bias shown in Fig.5 can be due to an instrumental offset c^i_{kn}, or due to radar clutter c^c_{kn} (clutter = echo from a fixed target). All these contributions are additive:

$c_{kn} = c^r_{kn} + c^s_{kn} + c^i_{kn} + c^c_{kn}$.

We have to take into account that each radar cycle yields two samples per range gate, namely k and k'. The samples of signal and clutter are shifted by 180° from k to k', because the phase $\varphi(t)$ of the transmitter was flipped by 180° (change $\varphi(t)$ by 180° in eqs. (3) and (4)). This can be accounted for by changing the sign of $c_{k'n}$ when averaging

$$\overline{c}_{k,k'} = \frac{1}{N}\sum_{n=1}^{N}(c_{kn}-c_{k'n})$$

$$= \frac{1}{N}\sum_{n=1}^{N}(c^r_{kn}-c^r_{k'n}+c^s_{kn}-c^s_{k'n} \quad +c^i_{kn}-c^i_{k'n}+c^c_{kn}-c^c_{k'n}) .$$

Since for the instrumental bias $c^i_{kn} = c^i_{k'n}$, it is eliminated by averaging. This is called instrumental-DC elimination (DC = direct current, better to say: constant voltage contribution).

Because of the transmitter phase flip: $c^s_{kn} = -c^s_{kn}$ and $c^c_{kn} = -c^c_{kn}$. Since the noise is independent from one to the next interpulse period, a change in sign of c^r_{kn} does not change its statistical properties. We thus obtain, since $k' \hat{=} k$:

$$\overline{c}_k = \frac{2}{N}\sum_{n=1}^{N}(c^r_{kn}+c^s_{kn}+c^c_{kn}) . \qquad (5)$$

This averaging, commonly called "preintegration", has become a standard process in MST radar operations. It yields preintegrated data samples $\overline{c}_{kl}$ (l=1,...,L) at the time $t_l = 2\cdot l\cdot N\cdot K\cdot \Delta t_s$ for the preintegration period $t_i = 2\cdot N\cdot K\cdot \Delta t_s = 2N\cdot T_{IPP}$.

If the summation in (5) extends over a time period $t_i = 2\cdot N\cdot T_{IPP}$, which is much longer than Δt_s, the high-frequency noise contribution vanishes. For an integration period $t_L = 2\cdot L\cdot N\cdot T_{IPP}$ (L>>N), which is much longer than τ_ξ, the signal contribution approaches zero since it is slowly fading in amplitude and phase. Only the clutter

contribution $\overline{c^c_k} = 1/L \sum_{l=1}^{L} \overline{c}_{kl}$ remains, since it is constant in amplitude and phase. This can be used to eliminate the clutter component by means of a digital high pass filter operation: $\tilde{\overline{c}}_{kl} = \overline{c}_{kl} - \overline{c}^c_k$. This operation is called clutter-DC elimination, and is done after the preintegration.

For the preintegration given by (5), the number N of added samples has to be carefully selected. It is evident from Fig.5 that the integration period has to be much shorter than the typical time scale of signal variations. Suppose the integration period would extend over a full cycle of the signal oscillation in Fig.5. The integration then would yield $\overline{x}=0$ and $\overline{y}=0$. As can be seen from the displacement of the average values (crossed circles), the signal amplitude will be generally attenuated due to the pre integration. In the spectral domain the amplitude attenuation factor F is given by $F(f)=\sin(\pi f N T_{IPP})/\sin^{-1}(\pi f T_{IPP})$. This effect of attenuation is also called the combfilter effect (Schmidt et al., 1979). The sin Nx/sin x-function arises because a non-tapered, rectangular window is used. The advantage is that the processing can be made very efficient since no multiplication of the raw data series with a weighting function is necessary. As long as care is taken that the first zero crossing of F(f), which is at $f_N = 1/4NT_{IPP}$, is at a reasonably higher frequency than typical signal frequencies, F(f) can be used to correct the signal spectrum. After preintegration the maximum resolvable frequency f_{Dmax} (in section 2.2) has to be replaced by f_N.

It is also necessary that the real part x and the imaginary part y of the detected signal are correctly in quadrature (orthogonal). Ideally they must be phase-shifted by exactly 90° and must have equal amplitudes on the average. Accuracies of less than a few degrees phase difference and less than a few percent amplitude differenc are tolerable, however, and can be obtained by proper hardware adjustment. If these accuracies cannot be reached, a correction of the quadrature components can be applied within some limits (e.g., Röster and Woodman, 1978).

The preintegration of the quadrature components, formulated by (5), is normally done in a digital preprocessor, called adder or integrator (see Fig.3). Since this preintegration is a low pass filter process it can be done also in an analogue filter, as the clutter elimination which is a high pass filter operation. Obviously the digital processing is much more versatile and flexible. Both analogue and digital preintegration reduce the number of data samples by some orders of magnitude, and compress the huge data flow from the ADCs to make it managable for the host computer. This is the evident advantage of this preintegration process. It is often thought that this process also increases the signal-to-noise ratio since the voltages of the coherent signal but the power of the incoherent noise add. This leads to an improvement of the signal-to-noise (power) ratio by the factor N, since the noise bandwidth is changed by the factor N^{-1}. If one defines the noise in such a way that its bandwidth is equal to the signal-bandwidth, the preintegration process only reduces the wide noise-bandwidth to the acceptable limit close to the signal-bandwidth, and the signal-to-noise ratio does not

change by this preintegration. The advantage of this preintegration process is still the essential reduction of the number of raw data samples, without giving away information on the signal.

4.4 Coding

Another preprocessing step which is generally similar to preintegration is the decoding procedure (described in detail in the paper by Woodman, Sulzer and Farley in this handbook). The principle reason for applying coding/decoding (pulse compression) is to achieve a maximum average power at optimum resolution and maximum unambiguous range. A fairly low duty cycle of 0.1% and hence a low sensitivity would for instance result from using a single pulse of 1 μs duration (Δr=150m) and an interpulse period of 1000 μs (r_{max}=150 km). Increasing the pulse length to 32 μs would increase the duty cycle to 3.2%, but deteriorate the range resolution to 4.8 km. The range resolution of 150 m can still be achieved by phase-coding the transmitter pulse in time (lag) increments of, say 1 μs. The decoding has to be done by cross correlating the received complex time series c_k with the transmitted code s_m:

$$c^{j}_{k^*} = \sum_{m=0}^{M-1} c_{k^*+m} \cdot s_m$$

where M is the length of the code and k^* correponds to the range gate k at lag zero where the correlation function $c^{j}_{k^*}$ has a maximum. Thus, the decoding is nothing else but an integration over several range gate samples, which are multiplied by the weighting factor s_m.

The simplest and most versatile phase coding scheme is the binary code, where the phase is flipped between the two states -1($=0^{o}$) and +1($=180^{o}$). Since here the weights s_m are +1 or -1, the multiplication needed in the decoding process reduces to an addition/subtraction operation. For this reason the decoding can be done in a preprocessor similar to the hardware preintegrator described earlier, or the integrator/decoder can even be one unit. An advantage in MST radar applications is also that the decoding/integration processes are interchangeable, which reduces the number of operations by about two orders of magnitude (e.g., Woodman et al., 1980).

The best codes for radar applications obviously are those where sidelobes of the correlation function at $k^* \neq k$ are minimum. Reasonable sidelobe suppression is gained with Barker codes, where the phases are flipped in a sequence (e.g., +++++--++-+-+ for the 13-bit Barker code). The correlation function is 13,0,1,0,1,0,1,0,1,0,1,0,1. The best sidelobe suppression, achievable with a Barker code, is M^{-1}, and the sidelobes extend out to $M \cdot \Delta t_s$. Since the codes cannot be infinitely long, because the minimum range is extended with the length of the code, the sidelobe suppression of Barker codes is limited. The reason is that these sidelobes contain power from other range gates $k^* \neq k$, which cause ambiguities.

A better sidelobe suppression can be gained by application of quasi-random codes, which however need decoding before the preintegration. The most suitable codes for MST radar work are the complementary codes (e.g., Schmidt et al., 1979), which theoretically have no sidelobes within an interpulse period. A complementary code consists of a pair of two code sequences s_1 and s_2. These have the property that their correlation function sidelobes are exactly equal, but opposite in sign. Normally both code sequences are transmitted at one and the next interpulse period, and the range samples of these two periods are preintegrated and decoded separately. The coherent addition of the decoded sequences then yields the total elimination of the sidelobes ($k^* \neq k$) if the signal is coherent from one to the next interpulse period. The zero lag value $k^* = k$ contains the total signal amplitude. As an example: s_1=+++-++-+, s_2=+++---+-, yield the correlation functions c_1=8,-1,0,3,0,1,0,1 and c_2=8,1,0,-3,0,-1,0,-1 and the addition c_1+c_2=16,0,0,0,0,0,0,0. The peak value at $k^* = k$ is 2M. There is still the shortcoming of a long code, that it extends the shortest observable range. This can be overcome by transmitting a sequence of a complementary code and a short single pulse in one radar cycle.

5. Data Analysis

5.1 Correlation and spectrum analysis

After appropriate preintegration one still has to deal with the noise which is remaining within the bandwidth given by the signal. The elimination of the noise and further signal processing can be done in the time domain by covariance (correlation) analysis or in the frequency domain by spectrum analysis. Since the covariance function and the power spectrum are Fourier transforms of each other, both contain the same relevant information. Depending on the purpose and the feasibility of the analysis, either of both approaches, is used in practice (Rastogi and Woodman, 1974; Woodman and Guillén, 1974; Röttger and Schmidt, 1979; Schmidt et al., 1979; Carter et al., 1980; Clark and Carter, 1980; Sato and Woodman, 1980; Rastogi, 1983).

The complex autocovariance function of the quadrature components $\overline{c}(t)$ (preintegrated) is

$$\varrho(\tau) = \int \overline{c}(t) \cdot \overline{c}^{*}(t+\tau) dt,$$

where τ is the temporal displacement, and the * denotes the complex conjugate.
In digital form

$$R_k(\tau_j) = \frac{1}{L-j} \sum_{l=1}^{L-j} \overline{c}_{kl} \overline{c}^{*}_{kl+j} = \overline{\overline{c}_{kl} \overline{c}^{*}_{kl+j}} \quad , \; j=0,\ldots,J-1 \; , \; J \leq L,$$

where j is the lag parameter defining the lag $\tau_j = j \cdot t_i$.
For a fixed range k, $\overline{c}_l = \overline{x}_l + i\overline{y}_l$, and the covariance function becomes

$$R(\tau_j)=\overline{(\bar{x}_l\bar{x}_{l+j}+\bar{y}_l\bar{y}_{l+j})}+i\,\overline{(\bar{x}_{l+j}\bar{y}_l-\bar{x}_l\bar{y}_{l+j})}$$

$$= R_r(\tau_j)+i\,R_i(\tau_j)\,,$$

or $R(\tau_j)=|R(\tau_j)|\exp(i\phi(\tau_j))$

with $|R|=(R_r^2+R_i^2)^{1/2}$, $\phi=\arctan(R_i/R_r)$.

In radar applications the term correlation function is often used for $R(\tau_j)$ instead of covariance function. The correct definition of the correlation function $\varrho(\tau_j)$ is given by the normalized covariance function: $\varrho(\tau_j)=R(\tau)/|R(0)|$. As well as the autocorrelation function of the series $\bar{c}(t)$ we also compute cross-correlation functions for two different series, $\bar{c}_1(t)$ and $\bar{c}_2(t)$, in the spaced antenna applications.

The power spectrum is the Fourier transform of $\varrho(\tau)$, weighted by $W(\tau)$:

$P(\omega)=\int W(\tau)\cdot\varrho(\tau)\cdot\exp(-i\omega\tau)d\tau$

or in digital form

$$P_k(\omega_m)=\frac{1}{J}\sum_{j=0}^{J-1} W_j\cdot R_{kj}\cdot\exp(-i\omega_m\cdot j\cdot t_i)\,,$$

where W_j is an arbitrary weighting function (e.g., $W_j=J^{-1}$ for all j, etc.) and

$\omega_m = m\cdot\pi/J\cdot t_i$, $m = 0,\dots,J$, $t_i = 2N\cdot T_{IPP}$.

The first three moments m_0, m_1 and m_2 of the power spectrum yield the total signal power $\bar{P}$, the mean $\bar{\omega}_D$ of the spectrum, and the width $\bar{\omega}_w$ of the spectrum:

$$\begin{aligned}&\bar{P}=m_0=\int P(\omega)d\omega,\\ &\bar{\omega}_D=m_1/m_0,\ m_1=\int\omega P(\omega)d\omega\,,\\ &\bar{\omega}_W=(m_2/m_0-(m_1/m_0)^2)^{1/2},\ m_2=\int\omega^2P(\omega)d\omega.\end{aligned}\qquad(6)$$

Moments can also be deduced from the covariance function, which then yield the signal power, Doppler shift and spectral width, if the spectrum is symmetrical (Woodman and Guillén, 1974):

$$\begin{aligned}&\bar{P}=|R(o)|=R_r(o),\\ &\bar{\omega}_D=d\phi(o)/dt=\phi(\tau_1)/\tau_1,\\ &\bar{\omega}_W^2=2(1-|R(\tau_1)|/|R(o)|)/\tau_1^2.\end{aligned}\qquad(7)$$

The power $\bar{P}$ is a measure for the effective reflectivity, the Doppler frequency $\bar{\omega}_D$ determines the mean velocity, and the spectral width gives, after correction (e.g.

Hocking, 1983a), an estimate of the turbulent velocity fluctuations and the turbulence dissipation rate.

5.2 Parameter estimation

Before calculating the parameters $\bar{P}$, $\bar{\omega}_D$ and $\bar{\omega}_W$, the noise contributions have to be eliminated. The noise level can be estimated from a range gate where no signal is detectable, or from the same range gate when the transmitter is switched off. However, if the signal bandwidth is sufficiently narrower than the noise bandwidth the high frequency parts of the spectrum or the zero-lag value of $R_r(o)$ can be used to obtain the noise estimate. The latter estimate requires the interpolation of the signal covariance function from higher order lags to the zero-lag and the subtraction of the interpolated value from $R_r(o)$ to obtain the noise estimate.

The advantage of the correlation analysis is, that the power, the Doppler frequency and the signal coherency can be read directly from the autocorrelation function. The power $\bar{P}$ is the interpolated value of the real part of $R(\tau)$ at zero lag. If the imaginary part of $R(\tau>0)$ is zero, ϕ=const, $d\phi/dt=0$ and consequently $\bar{\omega}_D\hat{=}v'=0$. The amplitude $|R(\tau)|$, which is equal to $R_r(\tau)$ for $\bar{\omega}_D=0$, determines the persistency of the signal. The time lag at which $|R(\tau)|=0.5\cdot|R(o)|$ is called the statistical coherence time τ_ε, which is inversely proportional to the fluctuations of the radar signal. The deterministic coherence time τ_ε' is inversely proportional to the Doppler frequency $\bar{\omega}_D$ (given by the radial velocity). It is thus inversely proportional to $d\phi/dt$, which is essentially given by the imaginary part of the correlation function at small lags.

The uncertainty of the signal parameters depends on the number M·L of averaged samples and on the signal-to-noise ratio $SNR=\bar{P}/P_N$, where P_N is the noise power within a bandwidth equal to the signal bandwidth. Averaging over M samples of the correlation function or the spectra, which are computed from L preintegrated samples, is called postintegration. The fractional uncertainty of the power estimate is

$\varepsilon = \Delta\bar{P}/\bar{P} = (1+P_N/\bar{P})\cdot(M\cdot L)^{-1/2}$.

Say, the preintegration time was chosen to be t_i=1/3s, corresponding to a maximum noise (=signal) bandwidth of 3 Hz. Then a one minute postintegration corresponds to M·L=180. For SNR=1, this yields ε=0.15. To obtain the same uncertainty for SNR=0.1, the postintegration time t_p has to be 30 min, and for SNR=0.01, t_p=42h. The uncertainties of $\bar{\omega}_D$ and $\bar{\omega}_W$ depend in a similar way on $(M\cdot L)^{-1/2}$, e.g. Woodman and Hagfors (1969). However, it is questionable if postintegration times of more than several hours are reasonable, since the signal parameters are not stationary over such a long time period. These constraints of signal-to-noise ratio and signal stationarity place a definite limit on the sensitivity of radars (see section 9). Obviously, for SNR<<1 an increase of the transmitted power by a factor Q would reduce the postintegration time by Q^{-2} to obtain the same uncertainty ε. This is the essential point one has to bear in mind when discussing the sensitivity of radars; it is not so much the marginal increase of maximum

observable altitude by increased power but the improvement in time resolution.

The three parameters $\overline{P}$, $\overline{\omega}_D$ and $\overline{\omega}_w$ fully define a power spectrum with Gaussian shape

$$P(\omega) = \frac{\overline{P}}{\sqrt{2\pi}\,\overline{\omega}_w} \cdot \exp\left(-\frac{(\omega-\overline{\omega}_D)^2}{2\,\overline{\omega}_w^2}\right),$$

which is assumed to be a good approximation for many conditions. These parameters yield information on the radar reflectivity ($\overline{P}$), turbulence intensity ($\overline{P},\overline{\omega}_w$), mean radial velocity ($\overline{\omega}_D$) as well as the mean velocity fluctuations ($\overline{\omega}_w$) and the stability ($\overline{P},\tau_\varepsilon$) and persistency ($\overline{P},\tau_\varepsilon$) of layered structures in the radar volume. The parameters can be deduced either directly by applying equations (6) or (7), by parameter fitting or iteration procedures. Special circumstances, e.g. signal aliasing, variable interference, fading ground clutter, ocean clutter echoes or the simultaneously occurring echoes due to reflection and scattering, demand the application of special methods. These are, for instance, discussed by Röttger (1980b), Sato and Woodman (1980), Rastogi and Holt (1981), Rastogi and Röttger (1982), Hocking (1983 a,b).

6. Measurements of Velocities

Let us first discuss the measurements of the mean velocity since these are used to determine wind velocities in the atmosphere (e.g. Wilson and Miller, 1972, Gage and Balsley 1978). There are basically two methods to measure velocities with MST radars: One method uses a narrow radar beam swung into various directions and measures the Doppler frequency of the echoes scattered from irregularities. This method is the Doppler-beam-swinging (D.B.S.) method. Another method uses three or more spaced antennas, and the received signals are cross-correlated to determine the drift speed of the scattering/reflecting irregularities (Briggs, 1977; Röttger and Vincent, 1978; Vincent and Röttger, 1980; Röttger, 1981b). This method is the spaced-antenna-drifts (S.A.D) method. More often they are just called the Doppler and the spaced antenna (SA) methods. Both methods are schematically sketched in Fig.6.

6.1 Spaced antenna method

The spaced antenna method measures the temporal and spatial variations of the field pattern of the radar echoes with vertically beamed antennas. As the reflecting or scattering irregularities move through the beam they produce a moving diffraction pattern on the ground which is sampled at three or more spaced receiving antennas. By cross- correlating the received signals it is possible to measure the time delays τ_a, between the receiving antennas and hence the apparent velocity V_a. This can be corrected for random changes to give the so-called true velocity V_t (see Briggs, 1977, and this handbook for more details). The vertical velocity component is estimated from the complex autocorrelation or the spectral analysis.

When deducing the wind velocities from spaced antenna measurements, one assumes that the drifting irregularities are carried with the wind (Taylor hypothesis), which has been confirmed by comparing drift data with in-situ measurements.
Röttger and Czechowsky (1980) first presented results of simultaneous measurements with the spaced antenna and the Doppler method, which they also compared with parallel aircraft and radiosonde measurements. In Figs. 7a and 7b, examples of their comparisons with the spaced antenna method are shown, where $|u|=(U^2+V^2)^{1/2}$ is the speed and $\alpha=\arctan(-U/-V)$ is the direction of the wind, U and V are the zonal and meridional components. The aircraft measurements (a) were in a few kilometers distance from the radar, whereas the radiosonde measurements (b) were in about 100 km distance north of the radar. The aircraft and radar data are in excellent, and the radiosonde and radar data are in good agreement. Because the latter measurements were separated by more than 100 km, where the wind variability already causes considerable differences, the similarity of both these wind profiles is convincing. Of course, such comparisons have to be confined to the troposphere and lower stratosphere, but their very reasonable outcome gains confidence that wind measurements with this method are correct in the whole middle atmosphere (papers by Briggs, Fraser and Schminder in this handbook).
The comparisons of Röttger and Czechowsky (1980) showed also that the spaced antenna measurements are evidently competitive with Doppler measurements.

Since its introduction to VHF radars, it appeared that the spaced antenna method has advantages and disadvantages compared with other methods for measuring winds. Because of the aspect sensitivity, it was argued that the spaced antenna method is most suitable since it uses vertical beam antennas and one ne d not worry about sidelobe effects. Obviously an increase of the signal-to-noise ratio is gained and the fixed vertical beam positions are technically much easier to handle than steerable antenna beams. However, also the spaced antenna method needs signals which are scattered and diffusively reflected from off-vertical directions (Briggs, 1980). It is alsc evident that the field pattern on the ground depends on the degree of horizontal coherency of the reflecting structures as well as on the width of the transmitter and receiver antenna beams; i.e. a large structure coherency and large antenna apertures (narrow beams) cause large correlation distances of the ground field pattern. This places limits on the antenna size and separation. If, for instance, the correlation distance is much larger than the antenna separation, a very broad cross-correlation function ϱ_a will result, which increases the error in determining the lag τ_a. The optimum antenna spacings and sizes can be prescribed only if correlation times and distances as well as horizontal velocities are known. The best spacing of the receiving antennas would probably be such that the field pattern drifts from one antenna to the other in not less than some 10% of the correlation time τ_ϱ. Of course, the sampling rate of the signal has to be short enough to resolve the correlation time. Observed average values of τ_ϱ are mostly around one second, although much higher and much lower values can occur. Typical horizontal velocities are between some ms^{-1} to some ten ms^{-1} with average values around about 20 ms^{-1}. This yields an optimum spacing of several ten meters and places an upper limit to the antenna sizes, which in turn yields an upper limit of the sensitivity of a spaced antenna system. However, for high signal-to-noise ratios, which normally characterize signals from the troposphere and lower stratosphere, this antenna size limit does not impair the application of the spaced antenna method. It rather supports its application in small and cost-effective systems.

Of course, many more details, such as analyses procedures and data selection criteria, have to be considered when planning, designing and operating a spaced antenna system, and the reader is referred to the comprehensive papers by Briggs (1977,1980), Vincent and Röttger (1980), Röttger (1981b), Hocking (1983 c), Røyrvik (1983). It was recently accepted that an MST radar spaced antenna system can also be used in the interferometer mode, which yields additional useful information on spatial structures of waves and turbulence. The application of this technique is outlined in section 6.3.

6.2 Doppler methods

In contrast to the spaced antenna method, the Doppler method measures the Doppler shift of the scattered radar echoes at oblique incidence (Fig.6). The complex autocorrelation or the spectral analysis yields radial velocities V' at different pointing directions. Assuming that the antenna beam points at a zenith angle δ and at an azimuth angle α, directed clockwise from north, then

$$V' = U\cdot\sin\alpha\cdot\sin\delta + V\cdot\cos\alpha\cdot\sin\delta + W\cdot\cos\delta. \qquad (8)$$

For a constant zenith angle and if the wind field is uniform, V' will vary sinusoidally with the azimuth angle α. The Fourier analysis of the data series $V'(\alpha)$ directly yields the eastward wind U and the northward wind V from the Fourier coefficients, as well as the vertical velocity W from the constant offset. This is the so-called VAD method (velocity-azimuth-display).

This method can be simplified by using only three fixed beam positions, one at $\delta = 0^o$ and the other at a zenith angle $\delta \neq 0^o$ and two azimuth angles α, which preferably should be orthogonal to each other. We directly can solve (8) to obtain U, V and W after measuring V' at the three beam directions. A most simplified method uses only two beam directions at different azimuths and assumes that the vertical velocity is negligible. We will call these the fixed-beam-methods. Two or three fixed beam positions are mostly used in MST radar applications. With fixed beams, however, most preferably the vertical and off-vertical directions in four orthogonal azimuth directions at equal zenith angles should be used. This would allow to reduce errors due to non-uniformity and inclined structures as well as to measure uniquely the correlation $\overline{U'W'}$ of the horizontal and vertical velocities (see section 6.3).

To obtain a most accurate estimate of the vertical velocity W, a velocity-elevation-display (VED) can be used. Here the azimuth is kept constant and the elevation is changed from $+\delta$ to $-\delta$. A fit of the portion of the sinusoidal variation within these limits of δ to the data series $V'(\delta)$ yields $U\cdot\sin\alpha + V\cdot\cos\alpha$ and W. Extending this elevation scan to two azimuth directions, also U and V can be determined.

Further information on the VAD, VED and fixed-beam Doppler measurements can be found in Wilson and Miller (1972), Battan (1973), Koscielny and Doviak (1983), Strauch et al. (1983).

An example of a VED measurement with an MST radar is shown in the series of spectra shown in Fig.8 (from Röttger et al.,1981). The antenna beam (half power beam width= 1.7^o) was swung in the zonal plane ($\alpha = 90^o$) in zenith angle steps $\Delta\delta = 3.4^o$. The Doppler shift increases proportional to sin δ, which is obviously expected if the zonal wind component U is non-zero. The remaining Doppler shift at $\delta = 0^o$ (e.g. at 17.2 km) is due to a vertical velocity W. Evidently, the signal power decreases with δ, which indicates that the detected anisotropic structures are horizontally stratified. Within these limits of δ the signal power decreases about exponentially by 1-2dB/degree in the troposphere and by 2-3 dB/degree in the lower stratosphere. This effect is also called aspect sensitivity.

The spectral width $\bar{\omega}_w$ is a measure of the turbulent velocity fluctuations in the radar volume. However, it is diluted by the effects of beam width and wind shear broadening (e.g. Battan, 1973, Hocking, 1983a). The former occurs because the radial components of the wind velocity vary from one edge of the radar beam to the other. The effect of beam width broadening is the stronger the wider the beam width is. The latter occurs if a shear of the wind exists across the width of the beam or along the radial extent of the radar volume (because of the finite width of the range gate). Vertical wind shears or gradients additionally create an offset of the mean velocity if the extent of the range gate Δr is larger than the gradient scale length (Sato and Fukao, 1982).

The finite beam width also gives rise to errors in estimating the Doppler shift since the scattering/reflection process is not isotropic. The product of the antenna beam pattern with the angular distribution of the aspect sensitivity yields an effective beam direction which is closer to the zenith than the real pointing direction. This error is largest if a strong reflected component is observed and can result in a velocity underestimate of some ten percent. It can be minimized by applying the measured aspect sensitivity for correction. Even for scattering, a similar underestimate can arise if there are strong horizontal fluctuations of the wind velocity. Here the width of the spectrum depends on the zenith angle, and it can be shown (Hocking, 1983a,b) that the contributions from subvolumes at different zenith angles within the antenna beam result in a bias towards low frequency components of the spectrum, i.e. yielding an underestimated horizontal velocity. Depending on the direction and the suppression of antenna sidelobes, the spectrum will also be altered which results in errors of power, mean velocity and velocity fluctuations.

As a result of these considerations, the width of the antenna beam and of the range gate should be made as narrow as possible. Of course, the sampling rate has to be made short enough to resolve the full shift and width of the signal spectrum.

There are several reasons to choose the zenith angle δ of the antenna beam as small as possible: 1) The spatial uniformity of the wind field is better for smaller separations of the probed radar volumes. Deviations from uniformity cause a higher bias and variance of the velocity estimates, especially if only fixed beam methods are used (Koscielny and Doviak, 1983). 2) The altitude resolution Δz diminishes with increasing zenith angle δ. This is fairly pronounced for broad antenna beam widths. 3) Since the range r to a specified altitude increases with zenith angle, a loss of sensitivity results due to the r^{-2} dependence of the echo power. 4) The effective aperture decreases with zenith pointing angle for a fixed antenna aperture assembled in the horizontal plane. 5) The anisotropy of the scattering/reflecting process yields stronger echoes at near-zenith angles.

Other effects, however, support the choice of large zenith angles: 6) The uncertainty of the velocity estimate $\Delta V'$ decreases with increasing Doppler shift, because

the ratio $\bar{\omega}_D/\bar{\omega}_w$ decreases with δ (assuming that $\bar{\omega}_w$ varies less with δ than $\bar{\omega}_D$), and $\bar{\omega}_w$ is consistent with the variance of $\bar{\omega}_D$. 7) For a given $\Delta V'$, the uncertainty of the horizontal velocity is $\Delta V=\Delta V'/\sin\delta$. However, the larger the zenith angle the shorter the preintegration time must be chosen to avoid aliasing and comb-filter attenuation. 8) An instrumental error in the pointing direction causes larger deviations of the horizontal velocity estimate for small δ. 9) The effective pointing direction due to the aspect sensitivity is assumed to become negligible at large zenith angles where isotropic scattering will dominate.

In summarizing these arguments we find that a general proposal cannot be made to select an optimum pointing angle. As in the spaced antenna method (where one has to preselect antenna spacings) the beam pointing angles have to be preselected when applying the Doppler method. The application of either the spaced antenna and/or the Doppler method has advantages and limitations, and one has obviously to deal with a trade-off between accuracy, simplicity and cost-effectiveness when planning and operating an MST radar system.

Comparisons of Doppler wind measurements with rawinsondes were done with almost all existing radars. A fair too good agreement was always reported (e.g., Larsen, 1983c). As an example we show in Fig.9 comparisons of radar winds measured with the UHF radar at Arecibo and rawinsonde winds measured at San Juan. Fukao et al. (1982) state that most of the difference in the lower stratosphere can be explained by experimental errors, especially those of the rawinsonde. The difference in the upper troposphere wind data are explained by the spatial and temporal variations in the wind field. Fukao et al. come to the agreeable conclusion that UHF and VHF Doppler radar measurements of winds provide a greater frequency and accuracy than the use of conventional rawinsondes. We also have to add that these radars can measure the vertical velocity with better accuracy than the yet applied methods , which is of considerable interest to meteorologists.

6.3 Radar interferometry

Both, the Doppler and the spaced antenna drift method, do not separately evaluate the spatial distribution of the phases of the field pattern at the ground. With the spaced antenna set-up the amplitudes and the phases can be measured. Combining in a suitable procedure the complex signals from different antennas is in a wide sense the application of the interferometer technique. In the first spaced antenna measurements with VHF radars, Röttger and Vincent (1978) and Vincent and Röttger (1980) applied this method to measure the angular spectrum of tropospheric returns. It can be expected that further valuable additional information on structure shapes and motions as well as on atmospheric waves can be obtained with this technique.

An essential point which has to be stressed at first is the improvement of the vertical velocity measurements by using a spaced antenna interferometer. The basic principle of the technique is sketched in Fig.10. Let us assume diffuse reflection from

a rough surface or structure S which is sufficiently far from the radar antenna and which is slightly tilted to the horizontal by an angle δ'. This structure moves with a velocity given by the horizontal component U and the vertical component W. A radar with vertically pointing antenna A_o with beam width larger than δ' measures the radial velocity

$$V' = W^* - U^* = W \cdot \cos\delta' - U \cdot \sin\delta'.$$

Thus, even when knowing the horizontal velocity U, the vertical velocity is still incorrect, if δ' is unknown (Röttger, 1981c).

The reflected signal can also be received at two separate antennas A_1 and A_2, and the complex cross correlation function ϱ_{12} be computed. Its amplitude $|\varrho_{12}|$ and phase ϕ_{12} is sketched in the lower part of Fig.10. From the displacement τ_{12} of the maximum of $|\varrho_{12}|$ and the horizontal separation d_{12} of the receiving antennas, the apparent velocity $V_a = d_{12}/2\tau_{12}$ is calculated. We assume here for simplification that V_a=U (instead of V_a, the true velocity has to be calculated according to the considerations in section 6.1 and Briggs in this handbook). The radial velocity is calculated from the time derivative of ϕ at τ=0:

$$V = \lambda_o/4\pi \cdot d\phi(o)/dt.$$

The tilt angle δ', which is similar to the incidence angle δ, is

$$\delta' = \arcsin(\phi_{12}(0) \cdot \lambda_o/2\pi d_{12}),$$

This yields the corrected vertical velocity

$$W=(V'+V_a\sin\delta\ )/\cos\delta\ .$$

For a typical ratio U/W=100 and δ=0.6°, for example, the vertical velocity estimate would be incorrect by a factor of 2 (0.5) if this correction were not applied.
The angle δ' is equivalent to the inclination the reflecting strutures. Its average can give an estimate of the inclination of isentropic surfaces (baroclinicity), which is evidently of interest for meteorological applications (Gage, 1983).

A phase lag between two antennas can also be introduced instrumentally, either by including a delay line between the antennas and the receiver or by adding a phase lag to the complex signal samples received at the different antenna channels. In the first case (preselected beam direction) the signals from both antennas would be added in an analogue coupler, and in the second case (post-selected beam direction) the digital samples would simply be added as vectors during data processing. This procedure is equivalent to electrically swinging the beam to different angles δ. The addition (distribution) of signals from (to) different antenna moduls is used to swing the receiver (transmitter) beam of a phased array. For separate transmission and receiving antennas, the transmitter antenna beam can be kept fixed and the receiving antenna beam be swung by post-selection as long as the angle δ is narrower than the beam of the transmitter antenna. The advantage of this latter method is the post-selection of all

possible angles δ, whereas the former method preselects an angle which cannot be changed after the data were taken. Of course, this method is easily extendable from the explained 1-dimensional example to a 2-dimensional application as well as to an array of more than two antenna modules.

This radar interferometer method allows not only the measurement of the horizontal wind components by the Doppler method, but also the tilt, the aspect sensitivity and the horizontal phase velocity and wavelength of atmospheric waves.

Vincent and Reid (1983) applied two symmetrical fixed beam directions at zenith angles δ and $-\delta$ with an HF radar to study mesosphere dynamics. They showed that this generally allows measurement of the cross correlation $\overline{U'W'}$ of the fluctuations W' and U' of the vertical and horizontal velocities, respectively:

$$\overline{U'W'} = \left(V'^2(\delta) - V'^2(-\delta)\right)/2 \sin 2\delta.$$

It is evident that this comprises a very powerful tool to measure gravity wave parameters and momentum flux, which is proportional to $\overline{U'W'}$.

Originally, Vincent and Reid used two fixed transmitter/receiver antenna beams. It is also possible to apply the method of post-selecting the receiver beam directions. This is illustrated by one example shown in Fig.11. Here the beam of the spaced receiving antennas of the SOUSY-VHF-Radar was "steered" to δ=+1.2° and δ=-1.2° by digitally inserting a phase delay to the recorded data. This allowed observation of two different phase locations of a wave in the stratosphere, which becomes clear due to the phase shift between the two time series of the displayed radial velocity. From these measurements, either by using post- or preselected beam directions, the horizontal wavelength and phase velocity, the momentum flux and the mean horizontal and vertical velocities can be deduced. The full 3-dimensional information has to be obtained by steering the antenna in two orthogonal vertical planes. The vertical wavelength and phase velocity can be found from just one, preferably vertical beam direction.There are also influences on spectral width and received power due to gravity waves, which were analyzed by Gage et al. (1981).

Another application, which originally was used to study ionospheric plasma turbulence (Farley, et al.,1981), was recently also applied to MST radars to trace discrete structures, such as blobs of turbulence moving through the antenna beam. (Röttger and Ierkic, in prepartion). By making use of a cross spectrum analysis and observing the change of δ and V' as a function of time, not only the location of the blobs but also their vertical and horizontal velocities can be measured more accurately.

The measurements of δ and its temporal variations are very useful to avoid erroneous interpretations that the radial velocities measured with vertical antenna beams are really vertical velocities. All these techniques, evaluating the temporal as

well as the spatial variations of amplitude and phase of the field pattern, we may call MST radar interferometry. Their applicability to MST radars has already been tested, but more refinement is needed to fully exploit this promising technique.

7. MST Radar Antennas

7.1 Basic parameters

The considerations on the interferometer applications can be extended into a brief description of antenna arrays (e.g., Skolnik, 1970). Assume that N individual antenna elements with equal spacing d are horizontally lined up to form a multi-element array. In the array far-field ($r > (N \cdot d)^2/\lambda_o$) the polar diagram is

$$E(\delta) = \sum_{n=1}^{N} E_n(\delta) \exp\left(i\left(\frac{2\pi(n-1)d}{\lambda_o} \sin\delta + \phi_n\right)\right) \qquad (9)$$

where $E_n(\delta)$ is the pattern of an individual element and ϕ_n is a relative phase placed on this element. Thus, the polar diagram is just the Fourier transform of the spatial aperture distribution. If all elements have similar $E_n(\delta)$ and ϕ_n, the polar diagram is a function sin Nx/sin x with $x = \pi d \sin\delta/\lambda_o$. If $d < \lambda_o$, there is only one main lobe at $\delta = 0^o$ (for $\phi_n = 0$). If $d > \lambda_o$, grating lobes at $\delta_G = \arcsin(\lambda_o/d)$ occur, for $E_n(\delta) = \text{const}$ with amplitudes similar to the main lobe. The width of the main lobe is $\delta_B = \arcsin(\lambda_o/Nd)$. In some radar applications also the two-way beam width $\delta_B/\sqrt{2}$ is used. If δ_B is small, it is directly proportional to the ratio of the wavelength λ_o to the aperture dimension $N \cdot d$. Nulls of the radiation pattern are at $\delta_n = \pm\, n \cdot \delta_B$, where $n = 1, 2, \ldots, N/2$, and sidelobes occur at $\delta_s = \delta_n \pm \delta_B/2$. If equal weighting W_n is applied to each of the single elements (e.g., $E_n(\delta) = W_n \cdot E_n'(\delta)$, with $W_n = \text{const}$ for all n), the first sidelobe closest to the main lobe is suppressed by 13.2dB.

The antenna pattern, namely the direction δ_o of the main lobe, can be changed by applying a linearly progressing phase ϕ_n from element to element, which has to be $\phi_n = 2\pi d(n-1)\sin\delta_o/\lambda_o$.
This beam steering should be within reasonable limits of the individual element pattern $E_n(\delta)$ to avoid undesirable degrading of the antenna radiation.

To obtain improved sidelobe suppressions, a tapering of the antenna array can be applied by either changing the weighting function W_n (electrical weighting, i.e. feeding the outer elements of an array with less power than the inner elements), or by using unequal element spacings d_n (spatial weighting, i.e. applying larger spacings for the outer elements). The price one has to pay for the improvement of sidelobe suppression by tapering is always a broadening of the main lobe and a lowering of the antenna gain G. Using a triangular weighting, for instance, improves the sidelobe suppression to -26 dB, but widens the main lobe by a factor of 1.44 and reduces the gain by 25%, as compared to uniform weighting. The respective values for a $\cos^2$-weighting, which is a good approximation to a Gaussian weighting, are -32 dB, 1.64 and 33%.

These 1-dimensional considerations can easily be extended to a realistic 2-dimensional radar antenna array by using, instead of d, the projections d' of all element positions onto an axis elongated in the azimuth direction α. The total antenna pattern then can be calculated by (9) for any α and δ. For a real radar antenna we also have to consider that the radiation can be into only one half sphere. For an array system this means that reflections from the ground, a screen or reflector elements have to be included in the calculations.

The antenna gain G is defined as the ratio of the maximum radiation intensity (in the main beam) to the average radiation intensity (averaged over all δ and α). For an antenna array with reasonable sidelobe suppression it is given by the antenna area or approximately by the inverse of the two orthogonal beam widths δ_B' and δ_B'' (in radians):

$$G = \frac{4\pi A}{\lambda_o^2} \approx \frac{4\pi}{\delta_B' \, \delta_B''} , \qquad (10)$$

The effective area A or aperture of the antenna is the product of the physical area of the antenna and the efficiency of its illumination, which for instance may be reduced by tapering. It is noted that A does not include the losses of the antenna and its feed system.

The considerations of antenna arrays, consisting of several discrete elements, can generally be extended also to antennas with continuous aperture illumination, such as dish antennas. The aperture A of a phased array or a dish antenna is used to calculate the power-aperture product $P \cdot A$, which defines the sensitivity of an MST radar. Note that P is the effective average power, which is radiated by the antenna, i.e. it is smaller than the output power of the transmitter due to losses in the antenna and feed lines.

This very brief outline is useful to estimate some basic values needed to plan and design a VHF-radar antenna system. The minimum requirement for investigations of the troposphere and stratosphere is a power aperture product $P \cdot A = 10^6\ \text{Wm}^2$ (see Fig.15). We assume that the radar sensitivity is a function of A^k, where $1 < k < 2$ depending on the reflected contribution (see equation (1)). It means that in practice one should favour an extension of the antenna area against an increase of the transmitter power. For a commonly achievable transmitter power $P = 10^3$W, $P \cdot A = 10^6\ \text{Wm}^2$ yields the dimension of a circular antenna array to be about $N \cdot d \approx 36$ m. For $\lambda_o = 6$m we can obtain a half-power beam width $\delta_B \approx 9^o$, and a gain $G \approx 27$dB. This estimate assumes that the array is optimally filled with elements. A single dipole element over a proper reflector screen has an effective area of about 15 m^2 (at $\lambda_o = 6$ m). Thus, about 64 dipoles are needed to fill

the array. For a square array with 8x8 elements the resulting spacing is $d \approx 0.75\ \lambda_o$, and a grating lobe will not occur. The first nulls are at $\delta_n = \pm 9^o$, and the first sidelobes at $\delta_s = \pm\ 13.5^o$. To use such an array with the Doppler method, the antenna beam has at least to be steered to a zenith angle $\delta_o = 9^o$ to place a null into zenith direction (minimizes influences of aspect sensitivity). Even then a sidelobe at -4.5^o is a problem.

7.2 Sidelobe effects

When designing an MST radar antenna one has to trade between the choices to optimize the effective aperture or to optimize the sidelobe suppression. An optimization of the aperture increases the sensitivity. Suppression of sidelobes by tapering, attenuates undesirable signals which spoil the estimates of reflectivity and velocity. Generally, any sidelobe effects are equivalent to a broadening of the antenna beam. The return signal is due to a product of the antenna pattern with the varying atmospheric reflectivity structures. Thus, knowing the antenna pattern, it is in principal possible to find the signal spectra, which however may be a tedious computational and ambiguous procedure.

For vertically pointing main beams the sidelobe effects are efficiently suppressed because of the aspect sensitivity. It follows that sidelobes are a minor problem for spaced antenna methods. However, they can be crucial for Doppler methods, which need off-vertical beams. If a sidelobe is pointing towards the zenith a larger power may be received from the vertical than from off-vertical directions but quantitative estimates of this effect are not yet known.

To get an error estimate of sidelobe effects with an off-vertical main beam, we discuss the following 1-dimensional example. This yields a reasonable estimate since the sidelobe closest to zenith, in the plane in which the main beam is steered, mostly dominates the errors. For simplification we also assume that the width of the main beam and sidelobes are much narrower than the chosen off-zenith pointing angles. The general outcome of the error estimates, however, will not considerably be altered for wider antenna lobes.

Let P_1 be the power gain of the main lobe at δ_1, and P_2 the power of a sidelobe at δ_2. The aspect sensitivity shall be given by $a(\delta)$, and the radar detected structures shall move with a horizontal wind $-U$. Then equations (6) or (7) yield:

$$\overline{P} = a_1P_1 + a_2P_2,$$

$$\overline{\omega}_D = \overline{\omega}_1 a_1P_1/(a_1P_1+a_2P_2) + \overline{\omega}_2 a_2P_2/(a_1P_1+a_2P_2).$$

With $a_{1,2} = a(\delta_{1,2})$ and $\overline{\omega}_{1,2} = 4\pi/\lambda_o\ U \sin \delta_{1,2}$, we obtain the fractional errors $\Delta\overline{P}$ and ΔU, if one would neglect the sidelobe effects:

$$\Delta\overline{P} = (\overline{P} - a_1P_1)/a_1P_1 = a_2P_2/a_1P_1$$

and

$$\Delta U = (\overline{\omega}_D - \overline{\omega}_1)/\overline{\omega}_1 = (a_1P_1 + a_2P_2 \sin\delta_2/\sin\delta_1)/(a_1P_1+a_2P_2) - 1.$$

Using for example $\delta_1 = 9^o$, $\delta_2 = -4.5^o$ (without considering the apparent beam direction), $P_1 = 1.0$, $P_2 = 10^{-2}$ (for a worst estimate of -20dB two-way beam sidelobe suppression) and $a(\delta) = 1$ dB/degree corresponding to $a_1 = 1.3 \cdot 10^{-1}$ and $a_2 = 3.6 \cdot 10^{-1}$, yields $\Delta P = 2.8 \cdot 10^{-2}$ and $\Delta U = 4.3 \cdot 10^{-2}$. This means that the power would be overestimated by 2.8%, and the horizontal velocity would be underestimated by 4.3%. A similar computation will yield the error estimates for the spectral width. Since δ and $P_{1,2}$ are known instrumental parameters and $a(\delta)$ is fairly well known from observations, $\Delta\overline{P}$ and ΔU can be used for correction, which will yield a very reasonable estimate of $\overline{P}$ and U. It, thus, may appear to be more feasible to apply corrections, (which however have to take into account the two dimensional pattern) than use tapering. However, situations may occur (e.g., strongly tilted, reflecting layers), which would lead to substantial contributions through antenna sidelobes. These situations need special attention during the data analysis.

Also sidelobes at low elevation angles have to be considered since these cause strong echoes from the non-atmospheric targets in the surroundings of the radar antenna. It can be shown that the ground reflection very effectively cancels the radiation at grazing angles ($\delta \gtrsim 85\text{-}90^o$), because the reflected wave suffers a phase reversal during reflection. This even can suppress low sidelobes of the array pattern which may be regarded as crucial without taking into account ground reflections. The location of an array antenna at a flat ground (extending out to several 100 m) may be sufficient but a shallow valley generally should be prefered to further suppressing the low angle radiation effects. However, high extending targets, such as radio towers or mountains in the closer vicinity, will still cause considerable clutter echoes, even when optimizing the antenna array for low angle radiation suppression.

7.3 Antenna types and feed systems

VHF radars generally operate with quasi-vertical beams, i.e. the zenith angles are smaller than about 20^o-30^o. For MST work linear polarization is sufficient. Essentially four different types of antenna systems are in use: dish antennas, dipole arrays, coaxial-collinear arrays (coco) and Yagi arrays (e.g. Fig.12).

Dish or cylinder antennas are rarely used for VHF radar applications because of their large dimensions (NAIC,1976; Röttger et al., 1981; Hagfors et al.,1982). Only one or a few elements are applied as primary feed antennas. The beam steering is done either by moving the position of the feed antenna or the entire dish. This has the advantage that no complicated power distribution and phasing network has to be used to feed the antenna. Because of the limited size of the primary feed antennas, the low-angle sidelobe suppression is not sufficient, which results in strong clutter echoes.

All other phased array antennas consist of many single elements which have to be fed by a cascading network of cables, hybrids and phase shifters. The coco-antenna (Ochs, 1965; Balsley and Ecklund, 1972) has the advantage that the feeding of elements in one line is just done by interchanging the inner and outer conductor of a coaxial cable every half wavelength. The outer conductors of the aligned cable act as collinear dipoles. The feeding is done from the centre of a line, which may typically consist of 16-48 dipoles. Positioning several of these strings or rows in parallel at spacing $d<\lambda_0$, and feeding these by a suitable matching network results in a coco-array. The radiation and the losses in a coaxial string comprise a natural tapering, suppressing sidelobes in the plane of the string. Because the phase relation along a string is fixed, a beam steering parallel to the coco-string is not possible. Beam steering is achieved by inserting appropriate phase delays in the cables feeding the parallel rows. The coco dipoles have to be lined up a quarter wavelength over reflector wires or screens. This antenna type is cheap, because coaxial cable is used for antenna elements and the matching network is simple. The successive phasing from one collinear element to the next, however, degrades the bandwidth of this antenna type. Instead of coaxial cable as radiator, half wave dipoles can also be used which are fed in a properly adjusted phase to form a collinear antenna. The application of collinear dipole lines limits the steerability of an array, and for this reason frequently three antenna arrays are used with three different fixed beam directions (see Green et al., 1975; Balsley et al., 1980).

Single dipole or Yagi antenna elements, forming an array, are fed by a cascading network of open wire or coaxial cable systems (e.g., Czechowsky and Meyer, 1980, Czechowsky et al., 1984). The cascading is most appropriately done in 2^n branchings ($n=1,2,\ldots$). By these means one can feed parts of the antenna array with 1/2, 1/4,... power to provide tapering without dissipating power. The branching is best done in couplers, power dividers or hybrids, which prevent power, reflected from a mismatch, to return to the transmitter, and also minimize effects due to mutual coupling between the single antenna elements. The coupling can be critical if phase control is applied to steer the antenna beam. The phase control is usually inserted close to the final elements, which may be connected to form modules of 4 or 16 elements. For continuous beam steering, phasing is most easily done by inserting discrete phase delays in steps of $2\pi/16$ with a binary phase shifter. This can be achieved by only four relays, switching phases of 22.5°, 45°, 90° and 180°. The advantage of Yagi against dipole antenna elements is that no ground screen is needed because of the Yagi reflector. The multi-element structure of a single Yagi allows for a higher gain (improving the filling factor of an array) and a negligible coupling (<-25 dB) between adjacent Yagi-antennas in an array. Mostly Yagi antennas can be constructed in such a way that the bandwidth is several megahertz. The bandwidth limiting factors in a Yagi system essentially are

the phase-shifters. The losses of a Yagi system are also considerably lower than those of a coco-antenna. However, such a Yagi system is obviously more expensive than a coco-system. The feeding of an array system can be from one transmitter, but also sub-modules can be fed separately by several phase-controlled transmitters (Fukao et al., 1980). The transmitter phase control can even be used to steer the antenna beam. This, however, needs a similar phase control of the receiver channels.

8. MST Radar Equipment

8.1 Transmit-receive system

Separate antenna arrays can be used for the transmission and for the reception mode, but it is more effective to use only one antenna for both modes. While separate antenna arrays allow for sufficient decoupling of the receiver from the transmitter a fast and highly insulating transmit-receive duplexer has to switch the antenna from the transmitter to the receiver and vice versa, if only one antenna is used. The response and recovery time of the duplexer should be in the order of the range sampling time, i.e. typically less than 10 µs. To insulate a peak transmitter pulse amplitude of 10^5 W to a fraction of a Watt, which will not destroy the receiver, the decoupling attenuation has to be better than 60 dB. These specified values can be obtained with pin-diode hybrid switches. For more details, the reader is referred to the technical report by Czechowsky and Meyer (1980), where also more details on power distribution, phasing and antenna diagram calculations can be found.

A block diagram of a typical transmitter/receiver system of a VHF radar is shown in Fig.13. It depicts the design of the portable SOUSY Mini-VHF-Radar which was operated at the Arecibo Observatory (Röttger et al., 1981). According to individual requirements, many variations and modifications of such a system can be done, but Figs.13 and 14 describe a generally adopted design, basing on the outline of Fig.3. The 120 MHz signal of the master oscillator (MO) is divided by four to obtain a 30 MHz intermediate frequency, which can be modulated (MD) in amplitude (on/off) and phase ($0^\circ/180^\circ$). This is to provide phase coding and DC-elimination. A similar divider generates the 0° and 90° signals, which are necessary for quadrature detection. The operational frequency 46.8 MHz is generated by mixing with the local oscillator (LO) signal at 76.8 MHz. It is amplified in the transmitter (TX) and fed through the transmit-receive duplexer (TRX) and a reflectometer to the antenna. The signal received at 46.8 MHz is amplified in the receiver (RX), mixed with the LO-signal to an intermediate frequency (IF) of 30 MHz, and mixed down to the baseband in the quadrature detector (X). The two quadrature outputs, the real part (Re) and the imaginary part (Im), are low pass-filtered (LP) to match the receiver bandwidth to the bandwidth of the transmitted pulse.

There are some basic system specifications: The stability of the oscillators should be better than 10^{-4} Hz/ms to allow a good accuracy of coherent detection. The transmitter peak power typically is between 1 kW and 1 MW with duty cycles up to several percent. The transmitter bandwidth must cover the shortest pulse length of 1 µs (=2 MHz bandwidth). The transmitter is normally operated in class-C mode to gain an optimum efficiency.

The receiver noise figure need not be better than a few dB (some 100K), since the sky noise level (> 1000K) determines the sensitivity. A noise calibration signal (CAL) of 1000K, say, should be injected into the receiver front-end in order to provide an absolute power calibration (which also needs a continuous monitoring of the transmitter power). The receiver linearity range shall exceed 60 dB in order to avoid saturation with strong clutter signals. The phase flip and the quadrature detection must be within less than a few degrees accuracy, and the amplitude ratio of the quadrature components must not deviate from unity by a few percent. Of course, the receiver base-bandwidth (postdetection) has to be about 1 MHz to allow detection of the shortest pulses. Bessel filters are usually used as low-pass or post-detection filters.

8.2 Radar control and data acquisition

The control pulses for the transmitter/receiver and the ADC are generated in the digital part of the system where also the data acquisition takes place (Fig.14). In the displayed example no host computer is used. The system is simply controlled by preselected instructions from programmable read-only memories (PROMs) and by external settings. The dashed lines enclose those subunits of instructions, commands and data transfer which also could be executed more flexibly by a host computer. Typically the radar controller generates pulse trains of control pulses such as demonstrated in this example:

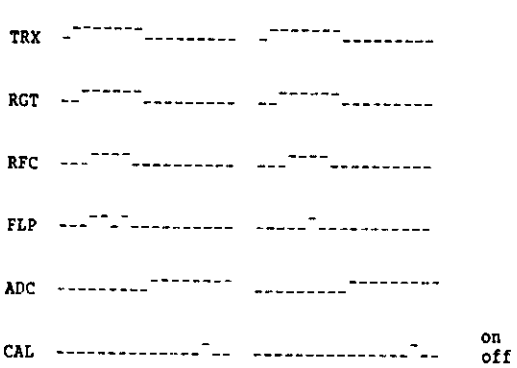

The transmit-receive duplexer (TRX) is switched on first, followed by a receiver gate pulse (RGT) and the switch-on of the transmitter radio frequency (RFC), which is phase flipped (FLP) between 0^{o} to 180^{o} for coding. The analogue-digital-converter starts

sampling (ADC) after RFC off and the TRX and RGT have opened the receiver. At the sixth sampled range gate a calibration signal (CAL) is injected. The whole sequence is repeated after one interpulse period when only the phase flip is inverted (for DC-elimination). For application of the complementary coding scheme a second double pulse code (consisting of the complementary pattern) is transmitted, and this radar cycle is repeated N times to yield one radar burst (section 4.2). Additionally, pulses for antenna control and other purposes can be generated, changing from one to the next radar burst. In more advanced systems multichannel receivers and ADCs are used (e.g. spaced antenna parallel processing, e.g. Röttger, 1981a). It is generally found that 8-bit ADCs are sufficiently matched to the linearity range of the receivers (>60 dB). If strong clutter signals are present the capacity must eventually be extended to 12 bit or a range dependent attenuation has to be used. Applying an 8-bit ADC and a 16-bit integrator allows to add samples from at least N=256 radar cycles in one channel (see section 4.3). The preintegration time then would be $t_i = 2N \cdot T_{ipp} = 128$ ms for $T_{IPP} = 250$ µs, corresponding to a maximum unambiguous range of 37.5 km and a maximum resolvable radial velocity of $12\,ms^{-1}$ ($f_{Dmax} = 4$ Hz). Applying a 4-bit complementary code and 300 m range resolution would result in a transmitter duty cycle of about 3%.

The radar operation, which is synchronized, started and stopped by external clock control, takes place in several nested sequences (section 4.): (1) the radar cycle, i.e. the transmission of one code unit of radar pulses with preselected duration and the sampling of the real and imaginary signal at preselected range gates (e.g. 128), (2) the integration cycle (burst), i.e. the repetition and coherent integration of an externally selected number of radar cycles, (3) record cycle, i.e. the repetition of a preselected number of integration cycles (e.g.64) to form one total record which is stored in a 16k memory. After completion, the memory content (pre-integrated raw data) as well as other parameter information (tape code, time etc.) are dumped in one tape record. The data analysis can be done off-line with a separate computer. This versatile device of a VHF radar transmitter/receiver, radar control and data acquisition system is housed in four small cabinetts, and with a suitable antenna array forms a complete operational VHF radar. Additionally, a hardware decoder, correlator or array processor can be attached (e.g., Woodman et al.,1980), and the whole system can be most flexibly controlled and monitored by a mini-computer, as done with most radars nowadays. This also would allow some real-time raw data display and analysis as well as automated real time transfer of meteorological parameters via a telephone modem. These expansions evidently depend on the individual necessities and requirements of the experimenters. The described mini-system, however, is already sufficient for a fairly optimized radar operation .

Descriptions of the early VHF radar systems were given by Woodman and Guillén, 1974; Green et al., 1975; Czechowsky et al., 1976; Röttger et al., 1978; Balsley et al., 1980), and design considerations were summarized by Balsley (1978a,b), Gage and

Balsley (1978) and Balsley and Gage (1982).

9. Sensitivity Requirements and Some Observational Examples

9.1 Empirical estimates

The sensitivity of a radar can be defined by the minimum detectable reflectivity. The detectability, which is the probability of discriminating a signal from noise, is given by the ratio of the average signal power to the noise power, multiplied by the square root of number of observations. The average signal-to-noise ratio (SNR) depends on the radar reflectivity and instrumental parameters and thus can be used to estimate the sensitivity of MST radars for a given number of data samples.

The noise in the lower VHF-band is essentially given by the sky noise. Depending on antenna beamwidth and direction as well as on time, the sky noise varies between about 1500K and 8000K at frequencies around 50 MHz.The noise power P_n is defined as the average power of sky noise within a typical signal bandwidth (here 3 Hz). The radar equation yields the signal power $\overline{P} \sim P \cdot A \cdot \Delta r \cdot C^2$, where $P=P_a$ (see section 2.3). The effective radar reflectivity C^2 and hence the signal power and sensitivity cannot easily be determined from theory, as was pointed out in earlier sections. We, thus, will use an empirical approach to determine the sensitivity of VHF radars, which can supplement the detectability estimate deduced by Gage and Balsley (1978).

In Fig.15 a typical tropospheric/stratospheric height profile of the signal-to-noise ratio SNR = $\overline{P}/P_n$ (in logarithmic units) is shown. Since SNR depends on the instrumental parameters P, A and Δr, the abscissa x has to be shifted accordingly. A useful way is to define the abscissa $x'=\log(P \cdot A \cdot \Delta r) - \log SNR$, since this directly allows to determine $\log SNR = \log(P \cdot A \cdot \Delta r) - x'$ for a given altitude z and given instrumental parameters P, A and Δr. These parameters are inserted in W, m^2 and units of 300m, respectively. The solid curve $\tilde{S}=z(x')$ directly yields the altitude z_o where the signal-to-noise ratio is unity; e.g., z_o=20 km for log $(P \cdot A \cdot \Delta r)$ =7, which can correspond to $P=10^4$W, $A=10^3$ m^2 and Δr=300 m.

The curve $\tilde{S}_o$ below 20 km was measured with the SOUSY-VHF-Radar in the spaced antenna mode (vertical beams). It represents an average over 290 hours of operation during 12 days between 28 Oct. and 12 Nov. 1981. This curve is characteristic for other VHF-radar observations in the middle latitudes. It shows the exponential lapse of received echo power with altitude and the typical increase of echo power above the tropopause. There are several regions with different echo lapse rate $\tilde{\Delta}=\Delta \log SNR/\Delta z$, these are: the lower troposphere (z<4 km) with $\tilde{\Delta} \approx -0.4$ km^{-1}, the middle and upper troposphere (4<z<10 km) with $\tilde{\Delta} \approx -0.5$ km^{-1}, the tropopause region (10<z<12 km) with $\tilde{\Delta} \approx +0.2$ km^{-1}, the lower stratosphere (12<z<25 km) with $\tilde{\Delta} \approx -0.25$ km^{-1} and the middle stratosphere (z>25 km) with $\tilde{\Delta} \approx -0.2$ km^{-1}. It cannot be excluded, however, that the middle stratosphere lapse rate is underestimated because of low signal-to-noise ratios of the measurements. The extrapolation of $\tilde{S}$ to larger altitudes than 20 km was done by using the lapse rates $\tilde{\Delta}$ from Rüster et al. (1980) and Balsley and Gage (1981).

Additionally, other limits are drawn in Fig.15. Since the signal power for reflection depends on A^k (1<k<2) instead of A, one expects for P·A=const a higher SNR if the ratio A/P increases. Thus, curves $\tilde{S}_o$,$\tilde{S}_1$ for two reasonable ratios A/P=0.1 (e.g. SOUSY) and A/P=1 (e.g. Jicamarca) are drawn. These two curves are valid only for quasi-vertical incidence. The aspect sensitivity $\overline{A}$ reduces the SNR for off-vertical beams, which yields the lower limit curve $\tilde{S}_2$. A zenith angle $\delta_o=7^o$ and an angular dependence of log SNR of 0.1/degree in the troposphere and 0.15/degree in the stratosphere is used; $\tilde{S}_3$ is for $\delta_o=15^o$.

Data points from other measurements taken at different radars with different zenith angles are included. Some uncertainty remains on these data points, since the exact average power aperture product and/or the noise bandwidth was not available. The different measurements also suffer from the varying noise level which yields an uncertainty in log SNR of about 0.4 units. However, the measured points generally confirm that the sensitivity relation given by $\tilde{S}$ in Fig.15 can be used as an average standard.

The mesosphere echoes (Czechowsky et al., 1979; Fukao et al., 1979; Ecklund and Balsley, 1981) are much more variable and cannot as easily be predicted; a brief description can be found in the following section and in Figs.16 and 19.

The effective reflectivity and hence the average sensitivity change due to variable strength of turbulence and refractive index structures, which depend on the meteorological conditions (e.g. Nastrom et al., 1982). Height variations of the tropopause, which may be as high as 18 km in the tropics, change the position of the secondary maximum around 10 km. The tropospheric reflectivity is higher when the humidity is increased. The average distribution of the logarithm of the reflectivity ($\hat{=}\log \overline{P}$) is in a good approximation log-normal with rms deviation σ_o. A height profile of σ_o is plotted in the left-hand corner of Fig.15, which was obtained from the 12 days observation period. It represents the general variability of the radar reflectivity, which decreases with height and is obviously higher in the troposphere (about $\pm$ 0.6 log-units) than in the stratosphere (about $\pm$ 0.3 log-units). The high σ_o-values in the lower stratosphere are due to the fact that the tropopause height is fairly variable.

9.2 Some typical MST radar records

Fig.15 shows profiles which were obtained by averaging over many days, but obviously also a seasonal variation occurs. This is depicted in Fig.16, where we notice that the upper stratosphere height of detectable signals is lower in summer than in winter. An explanation of this observation may be that the turbulence activity in the lower stratosphere differs with season (Balsley et al., 1983).

In Fig. 17 an example of the medium-term variability (period of a day) of reflectivity is shown, which is characterized by some relevant structures. This contour plot, which is discussed in detail by Röttger and Schmidt (1981) and Larsen and Röttger (1982), indicates the usefulness of VHF radar operations to observe the tropopause height and frontal boundaries. The reflectivity records combined with the observations

of aspect sensitivity and signal persistency allow to estimate the atmospheric stability (e.g., Gage and Green, 1979; Green and Gage, 1980; Röttger, 1980a) and to retrieve the temperature profile (e.g. Gage and Green, 1982; Westwater et al., 1983).

An impression on the signal variability at short-time and height scales can be obtained from the modified height-time intensity plot (Fig.18). This plot is obtained by suppressing the mean profile (average over many hours) and displaying only the residual power data. The thin structures, observed with vertical beam, are due to reflection from almost horizontal stratifications of refractive index changes. These are also called sheets or laminae because they are often even thinner than the normally applied range resolution of 150 m (Röttger and Schmidt, 1979). It is often found that they occur in multiples or patches which may be because they are signifying the outer boundaries of turbulence layers. They even indicate periodicities which can point out that they are connected with atmospheric wave structures. These sheets can gain a substantial increase in reflectivity by an order of magnitude or more. The fine-scale time variation of the sheets is characterized by coherence times of some seconds to some ten seconds.

The long-term variation of echoes from the mesosphere can be seen in the upper part of Fig.16. These continuous observations are from Pokerflat/Alaska at high latitudes (Balsley et al.,1983), and can be used also to estimate the detectability of mesospheric echoes as compared to tropospheric/stratospheric echoes. It was found here that there is a very marked change in the mesospheric echo height with season. In summer the echoes occur in the height range 80-100 km, whereas in other seasons the echoes range from about 55 to 80 km. The transition takes place abruptly in May and September. A similar seasonal variation of echo occurrence was also observed with the SOUSY-VHF-Radar (Czechowsky et al. 1979). Ecklund and Balsley (1981) reported that the peak signal-to-noise ratio is 1-2 orders of magnitude larger in summer than in autumn, and it even may occur that echoes are almost absent from January to March. It is assumed that the seasonal variation of the mesospheric echoes is possibly connected to the variable strength of turbulence. On the other hand, vertical gradients of electron density must be present. This connects the echo appearance to times when either high energetic particle precipitation enhances the electron density in the auroral mesosphere, or normally to the daylight hours. This diurnal variation is clearly depicted in Fig.19, which shows the mesospheric echo appearance for low latitudes (Arecibo/Puerto Rico). The mesospheric echo structures are also characterized by layers and sheets with different thicknesses and lifetimes (e.g., Czechowsky et al., 1979; Röttger, 1980). This makes it even more difficult to obtain a continuous altitude profile of echo power and wind velocity in the mesosphere. Additionally, meteor echoes can be observed between 90 and 110 km. These peak in the morning hours and also were used to measure wind velocitites (e.g. Avery et al., 1983). The time and height variability of mesospheric echoes makes it almost im possible at this time to predict the sensi-

tivity of VHF radars for operational studies of the mesosphere. A crude estimate can only be given (e.g.Fig.2), and we assume a power aperture product of 10^7 - 10^8 Wm^2 to be necessary for suitable mesospheric investigations.

10. Conclusion

During the recent years the number of MST radars has considerably increased, which proves the confidence in the application of this technique for remote sensing of the atmosphere. In Table 1 a summary of those radars is given which are operational, under construction or in a definite planning state. Also the incoherent scatter radars (IS) are included since all of them had been or will be used for ST work. Except of the Jicamarca radar, all IS radars operate at high VHF or UHF, and are not regular MST radars in terms of the definition of mesosphere-stratosphere-troposphere turbulence scatter. Some numbers of the technical parameters in this list (e.g., average power, min.pulse width, duty cycle, aperture and beam width) are uncertain to some extent, because either varying operation modes are used or these terms are defined in a slightly different manner according to the different experimenters' requirements. However, they give a gross overview and allow the determination of the minimum, average and maximum technical standard of the transmitter-receiver-antenna system. All these radars apply digital control, signal acquisition and processing. The radar controller is mostly a programmable hardware unit, whereas preprocessor (integrator, decoder, correlator, array processor) are either separate hardware units or implemented in the supervising host computer. The application of coding is not yet general standard but its implementation is often planned. The smallest radars, particularly those of the Platteville-type, operate only at a power-aperture product of 10^6 Wm^2 and detect echoes up to the lower stratosphere. The Jicamarca radar has the highest power-aperture product of $10^{10}Wm^2$, but its outstanding sensitivity is still barely sufficient to detect evaluable echoes from the gap region between 45 and 55 km altitude. A large international MST system is planned for operation close to the equator especially to allow the measurements of (vertical) velocities through almost the entire middle atmosphere (Balsley, private communication). This venture is of eminent interest for studying the dynamics of the middle atmosphere, particularly the global circulation pattern (e.g. Geller, 1979; Gage and VanZandt, 1981). One of the essential contributions of MST radars to dynamical meteorology of the middle and lower atmosphere is their capability to measure vertical velocities (e.g., Gage 1983). The determination of instrumental limitations and the development of optimum and error-minimized methods to measure the vertical velocity is still one of the outstanding tasks for the MST radar experimenters.

The evident capabilities of MST radars to investigate and monitor waves and turbulence and their mutual coupling with the mean flow of the general circulation pattern as well as the impact on vertical transport is recognized and accepted (e.g.,

Gage and Clark, 1978; Gage, 1979; Woodman, 1980; Klostermeyer, 1981; Lindzen, 1981; Woodman et al., 1981 ; Larsen et al., 1982). It is good exercise for the experimenters to fully develop existing as well as introduce new methods to measure whith optimum accuracy as many parameters of waves and turbulence as possible.

Finally, it shall be stressed here that the MST radar technique recently has developed into a state which allow its routine application for operational meteorology (e.g., Rötter, 1981a; Balsley and Gage, 1982; Hogg et al., 1983; Strauch et al., 1983 and Westwater et al., 1983). The capabilities of the MST radars to observe continuously the 3-dimensional wind field, frontal structures, the tropopause and static stability is more and more recognized (e.g., Lhermitte, 1979; Larsen and Röttger, 1982; Larsen, 1983b). The conclusive step-forward for the experimenter and system designer is to prepare MST radar equipment which operates continuously and unattendedly as well as to allow real-time analysis, access and transfer of relevant meteorological data.

Besides continuing to be used as very suitable research tools it now can be foreseen that within the next decade MST and ST radars may be linked in routine networks for real-time meteorological operations.

References

Avery, S.K., A.C. Riddle and B.B. Balsley (1983), The Poker Flat radar as a meteor radar (subm. to Radio Sci.).

Balsley, B.B. (1978a), The use of sensitive coherent radars to examine atmospheric parameters in the height range 1-100 km. Preprint Vol. 18th Conf. on Radar Meteor., 190-193 (publ. by Amer. Meteor. Soc., Boston, Mass.).

Balsley, B.B. (1978b), Design considerations for coherent radar systems for probing the troposphere, stratosphere, and mesosphere. Preprint Vol. 18th Conf. on Radar Meteor., 387-390 (publ. by Amer. Meteor. Soc., Boston, Mass.).

Balsley, B.B. and W.L. Ecklund (1972), A portable coaxial collinear antenna. IEEE Trans. Antennas Propag. AP-20, 513-516.

Balsley, B.B. and K.S. Gage (1980), The MST radar technique: Potential for middle atmospheric studies. J. Pure Appl. Geophys. 118, 452-493.

Balsley, B.B. and K.S. Gage (1981), On the vertical-incidence VHF backscattered power profile from the stratosphere. Geophys. Res. Lett. 8, 1173-1175.

Balsley, B.B. and K.S. Gage (1982), On the use of radars for operational wind profiling. Bull. Amer. Meteor. Soc. 63, 1009-1018.

Balsley, B.B., W.L. Ecklund, D.A. Carter and P.E. Johnston (1980), The MST radar at Poker Flat, Alaska. Radio Sci. 15, 213-223.

Balsley, B.B., W.L. Ecklund and D.A. Carter (1983), Capabilities and limitations of the Poker Flat MST radar. Preprint Vol. Workshop on Techn. Aspects of MST Radar, 23-27 May 1983, Univ. of Illinois, Urbana, Ill., paper 5.5-A.

Battan, L.J. (1973), Radar Observation of the Atmosphere. The Univ. of Chicago Press.

Bolgiano, R., Jr. (1968), The general theory of turbulence - Turbulence in the atmosphere. In: Winds and Turbulence in Stratosphere, Mesosphere and Ionosphere (edit. K. Rawer), pp. 371-400 (North-Holland Publ. Comp., Amsterdam).

Bowhill, S.A. (Edit.) (1984), Handbook for MAP, Vol. 9 (Workshop on Technical Aspects of MST Radar, 23-27 May 1983, Univ. of Illinois, Urbana) (publ. by SCOSTEP Secretariat, Univ. of Illinois, Urbana, Ill.).

Bowles, K.L. (1958), Observation of vertical-incidence scatter from the ionosphere at 41 Mc/sec. Phys. Rev. Lett. 1, 454-455.

Briggs, B.H. (1977), The analysis of moving patterns by correlation methods. Rpt. ADP 148, Dept. of Phys., The Univ. of Adelaide, Australia.

Briggs, B.H. (1980), Radar observations of atmospheric winds and turbulence: a comparison of techniques. J. Atmos. Terr. Phys. 42, 823-833.

Carter, D.A., B.B. Balsley and W.L. Ecklund (1980), The Poker Flat MST radar: signal analysis and data processing techniques with examples. Preprint Vol. 19th Conf. on Radar Meteor., 563-567 (publ. by Amer. Meteor. Soc., Boston, Mass.).

Clark, W.L. and D.A. Carter (1980), Real-time scaling of atmospheric parameters from radars using the MST technique. Preprint Vol. 19th Conf. on Radar Meteor., 599-604 (publ. by Amer. Meteor. Soc., Boston, Mass.).

Crane, R.K. (1980), A review of radar observations of turbulence in the lower stratosphere. Radio Sci. 15, 177-193.

Czechowsky, P. and K. Meyer (1980), Das Antennensystem des SOUSY-VHF-Radars. Rpt. MPAE-T-00-80-19, Max-Planck-Institut für Aeronomie, Katlenburg-Lindau, Germany.

Czechowsky, P., J. Klostermeyer, J. Röttger, R. Rüster, G. Schmidt and R.F. Woodman (1976), The SOUSY-VHF-Radar for tropospheric, stratospheric and mesospheric sounding. Preprint Vol. 17th Conf. on Radar Meteor., 349-353 (publ. by Amer. Meteor. Soc., Boston, Mass.).

Czechowsky, P., R. Rüster and G. Schmidt (1979), Variations of mesospheric structures in different seasons. Geophys. Res. Lett. 6, 459-462.

Czechowsky, P., G. Schmidt and R. Rüster (1984), The mobile SOUSY Doppler radar - Technical design and first results. Radio Sci. 19 (to be publ.).

Ecklund, W.L. and B.B. Balsley (1981), Long-term observations of the arctic mesosphere with the MST radar at Poker Flat, Alaska. J. Geophys. Res. 86, 7775-7780.

Farley, D.T., H.M. Ierkic and B.G. Fejer (1981), Radar interferometry: A new technique for studying plasma turbulence in the ionosphere. J. Geophys. Res. 86, 1467-1472.

Flock, W.L. and B.B. Balsley (1967), VHF radar returns from the D region of the equatorial ionosphere. J. Geophys. Res. 72, 5537-5541.

Fukao, S., T. Sato, S. Kato, R.M. Harper, R.F. Woodman and W.E. Gordon (1979), Mesospheric winds and waves over Jicamarca on May 23-24, 1974. J. Geophys. Res. 84, 4379-4386.

Fukao, S., S. Kato, T. Aso, M. Sasada and T. Makihira (1980), Middle and upper atmosphere radar (MUR) under design in Japan. Radio Sci. 15, 225-231.

Fukao, S., T. Sato, N. Yamasaki, R.M. Harper and S. Kato (1982), Winds measured by a UHF Doppler radar and rawinsondes: Comparisons made on twenty-six days (August-September 1977) at Arecibo, Puerto Rico. J. Appl. Meteor. 21, 1357-1363.

Gage, K.S. (1979), Evidence for a $k^{-5/3}$ law inertial range in mesoscale two-dimensional turbulence. J. Atmos. Sci. 36, 1950-1954.

Gage, K.S. (1983), On the measurement of vertical velocity by MST radar. Preprint Vol. Workshop on Techn. Aspects of MST Radar, 23-27 May 1983, Univ. of Illinois, Urbana, Ill., paper 3.4-A.

Gage, K.S. and B.B. Balsley (1978), Doppler radar probing of the clear atmosphere. Bull. Amer. Meteor. Soc. 59, 1074-1093.

Gage, K.S. and B.B. Balsley (1980), On the scattering and reflection mechanisms contributing to clear air radar echoes from the troposphere, stratosphere and mesosphere. Radio Sci. 15, 243-257.

Gage, K.S. and W.L. Clark (1978), Mesoscale variability of jet stream winds observed by the Sunset VHF Doppler radar. J. Appl. Meteor. 17, 1412-1416.

Gage, K.S. and J.L. Green (1978), Evidence for specular reflection from monostatic VHF radar observations of the stratosphere. Radio Sci. 13, 991-1001.

Gage, K.S. and J.L. Green (1979), Tropopause detection by partial specular reflection with very-high-frequency radar. Science 203, 1238-1240.

Gage, K.S. and J.L. Green (1982), A technique for determining the temperature profile from VHF radar observations. J. Appl. Meteor. 21, 1146-1149.

Gage, K.S. and T.E. VanZandt (1981), Wind measurement techniques available for the middle atmosphere program. J. Geophys. Res. 86, 9591-9598.

Gage, K.S., D.A. Carter and W.L. Ecklund (1981), The effect of gravity waves on specular echoes observed by the Poker Flat MST radar. Geophys. Res. Lett. 8, 599-602.

Geller, M.A. (1979), Dynamics of the middle atmosphere. J. Atmos. Terr. Phys. 41, 683-705.

Gossard, E.E. and R.G. Strauch (1983), Radar Observation of Clear Air and Clouds. Elsevier, Amsterdam, Oxford, New York.

Green, J.L. and K.S. Gage (1980), Observations of stable layers in the troposphere and stratosphere using VHF radar. Radio Sci. 15, 395-405.

Green, J.L., J.M. Warnock, R.H. Winkler and T.E. VanZandt (1975), A sensitive VHF radar for the study of winds, waves and turbulence in the troposphere, stratosphere and mesosphere. Preprint Vol. 16th Conf. on Radar Meteor., 313-315 (publ. by Amer. Meteor. Soc., Boston, Mass.).

Hagfors, T., P.S. Kildal, H.J. Kärcher, B. Liesenkötter and G. Schröer (1982), VHF parabolic cylinder antenna for incoherent scatter radar research. Radio Sci. 17, 1607-1621.

Hardy, K.R. (1972), Stucies of the clear atmosphere using high power radar. in: Remote Sensing of the Troposphere (edit. V.E. Derr), chapter 14 (Rpt. of Wave Propag. Lab., ERL, Boulder, Colorado, issued August 15, 1972).

Harper, R.M. and W.E. Gordon (1980), A review of radar studies of the middle atmosphere. Radio Sci. 15, 195-211.

Hocking, W.K. (1983a), On the extraction of atmospheric turbulence parameters from radar backscatter Doppler spectra - I. Theory. J. Atmos. Terr. Phys. 45, 89-102.

Hocking, W.K. (1983b), Mesospheric turbulence intensities measured with a HF radar at 35°S - II. J. Atmos. Terr. Phys. 45, 103-114.

Hocking, W.K. (1983c), The spaced antenna drift method. Preprint Vol. Workshop on Techn. Aspects of MST Radar, 23-27 May 1983, Univ. of Illinois, Urbana, Ill., paper 3.2-A

Hocking, W.K. and J. Röttger (1983), Pulse length dependence of radar signal strengths for Fresnel backscatter. Radio Sci. 18 (in press).

Hogg, D.C., M.T. Decker, F.O. Guiraud, K.B. Earnshaw, D.A. Merritt, K.P. Moran, W.B. Sweezy, R.G. Strauch, E.R. Westwater and C.G. Little (1983), An automatic profiler of the temperature, wind and humidity in the troposphere. J. Climate Appl. Meteor. 22, 807-831.

James, P.K. (1980), A review of radar observations of the troposphere in clear air conditions. Radio Sci. 15, 151-175.

Klostermeyer, J. (1981), MST radars: Advanced tools for gravity wave studies. Nature 292, 107-108.

Koscielny, A.J. and R.J. Doviak (1983), An evaluation of the accuracy of some radar wind profiling techniques. Preprint Vol. Workshop on Techn. Aspects of MST Radar, 23-27 May 1983, Univ. of Illinois, Urbana, Ill., paper 3.3-A.

Larsen, M.F. (1983a), The MST radar technique: A tool for investigations of turbulence spectra. Preprint Vol. Workshop on Techn. Aspects of MST Radar, 23-27 May 1983, Univ. of Illinois, Urbana, Ill., paper

Larsen, M.F. (1983b), The MST radar technique: Requirements for operational weather forecasting. Preprint Vol. Workshop on Techn. Aspects of MST Radar, 23-27 May 1983, Univ. of Illinois, Urbana, Ill., paper 1.1-A.

Larsen, M.F. (1983c), Can a VHF Doppler radar provide synoptic wind data? Preprint Vol. 5th Symp. on Meteor. Observations and Instrumentation, 183-190 (publ. by Amer. Meteor. Soc., Boston, Mass.).

Larsen, M.F. and J. Röttger (1982), VHF and UHF Doppler radars as tools for synoptic research. Bull. Amer. Meteor. Soc. 63, 996-1008.

Larsen, M.F., M.C. Kelley and K.S. Gage (1982), Turbulence spectra in the upper troposphere and lower stratosphere at periods between 2 hours and 40 days. J. Atmos. Sci. 39, 1035-1041.

Lhermitte, R. (1979), Advancements in remote sensing of the atmosphere. Rev. Geophys. Space Phys. 17, 1833-1840.

Lindzen, R.S. (1981), Turbulence and stress owing to gravity wave and tidal breakdown. J. Geophys. Res. 86, 9707-9714.

NAIC (1976), The users manual for the Arecibo Observatory. National Astronomy and Ionosphere Center, Arecibo Observatory, Arecibo, Puerto Rico, September 1976.

Nastrom, G.D., K.S. Gage and B.B. Balsley (1982), Variability of C_n^2 at Poker Flat, Alaska, from mesosphere, stratosphere, troposphere (MST) Doppler radar observations. Optical Engineering 21, 347-351.

Ochs, G.R. (1965), The large 50 Mc/s dipole array at Jicamarca radar observatory. NBS Rpt. 8772, National Bureau of Standards, U.S. Dept. of Commerce, Boulder, Colorado.

Rastogi, P.K. (1981), Radar studies of gravity waves and tides in the middle atmosphere: a review. J. Atmos. Terr. Phys. 43, 511-524.

Rastogi, P.K. (1983), Data processing techniques used with MST radars - a review. Preprint Vol. Workshop on Techn. Aspects of MST Radar, 23-27 May 1983, Univ. of Illinois, Urbana, Ill., paper 8.1-A.

Rastogi, P.K. and O. Holt (1981), On detecting reflections in presence of scattering from amplitude statistics with application to D region partial reflection. Radio Sci. 16, 1431-1443.

Rastogi, P.K. and J. Röttger (1982), VHF radar observations of coherent reflections in the vicinity of the tropopause. J. Atmos. Terr. Phys. 44, 461-469.

Rastogi, P.K. and R.F. Woodman (1974), Mesospheric studies using the Jicamarca incoherent-scatter radar. J. Atmos. Terr. Phys. 36, 1217-1231.

Röttger, J. (1980a), Structure and dynamics of the stratosphere and mesosphere revealed by VHF radar investigations. J. Pure Appl. Geophys. 118, 494-527.

Röttger, J. (1980b), Reflection and scattering of VHF radar signals from atmospheric refractivity structures. Radio Sci. 15, 259-276.

Röttger, J. (1981a), The capabilities of VHF radars for meteorological observations. ESA SP-165, 143-148 (publ. by European Space Agency, Paris).

Röttger, J. (1981b), Wind variability in the stratosphere deduced from spaced antenna VHF radar measurements. Preprint Vol. 20th Conf. on Radar Meteor., 22-29 (publ. by Amer. Meteor. Soc., Boston, Mass.).

Röttger, J. (1981c), Investigations of lower and middle atmosphere dynamics with spaced antenna drifts radars. J. Atmos. Terr. Phys. 43, 277-292.

Röttger, J. (1984), The MST radar technique, compared with the Thomson scatter radar technique - A comparison of coherent and incoherent scatter radars. EISCAT Techn. Rpt., EISCAT Scient. Association, Kiruna, Sweden (in preparation).

Röttger, J. and P. Czechowsky (1980), Tropospheric and stratospheric wind measurements with the spaced antenna drifts technique and the Doppler beam swinging technique using a VHF radar. Preprint Vol. 19th Conf. on Radar Meteor., 577-584 (publ. by Amer. Meteor. Soc., Boston, Mass.).

Röttger, J. and C.H. Liu (1978), Partial reflection and scattering of VHF radar signals from the clear atmosphere. Geophys. Res. Lett. 5, 357-360.

Röttger, J. and G. Schmidt (1979), High-resolution VHF radar sounding of the troposphere and stratosphere. IEEE Trans. Geosci. Electr. GE-17, 182-189.

Röttger, J. and G. Schmidt (1981), Characteristics of frontal zones determined from spaced antenna VHF radar observations. Preprint Vol. 20th Conf. on Radar Meteor., 30-37 (publ. by Amer. Meteor. Soc., Boston, Mass.).

Röttger, J. and R.A. Vincent (1978), VHF radar studies of tropospheric velocities and irregularities using spaced antenna techniques. Geophys. Res. Lett. 5, 917-920.

Röttger, J., J. Klostermeyer, P. Czechowsky, R. Rüster and G. Schmidt (1978), Remote sensing of the atmosphere by VHF radar experiments. Naturwissenschaften 65, 285-296.

Röttger, J., P. Czechowsky and G. Schmidt (1981), First low-power VHF radar observations of tropospheric, stratospheric and mesospheric winds and turbulence at the Arecibo Observatory. J. Atmos. Terr. Phys. 43, 789-800.

Røyrvik, O. (1983), Spaced antenna drift at Jicamarca, mesospheric measurements. Radio Sci. 18, 461-476.

Rüster, R. and R.F. Woodman (1978), Digital filtering, calibration and correlation analysis of radar-echoes from the tropo- and stratosphere. Kleinheubacher Berichte 21, 239-246 (publ. by Fernmeldetechnisches Zentralamt, Darmstadt, Germany).

Rüster, R., P. Czechowsky and G. Schmidt (1980), VHF-radar measurements of dynamical processes in the stratosphere and mesosphere. Geophys. Res. Lett. 7, 999-1002.

Sato, T. and S. Fukao (1982), Altitude smearing due to instrumental resolution in MST radar measurements. Geophys. Res. Lett. 9, 72-75.

Sato, T. and R.F. Woodman (1980), Spectral parameter estimation of cat radar echoes in the presence of fading clutter. Preprint Vol. 19th Conf. on Radar Meteor., 568-574 (publ. by Amer. Meteor. Soc., Boston, Mass.).

Schmidt, G., R. Rüster and P. Czechowsky (1979), Complementary code and digital filtering for detection of weak VHF radar signals from the mesosphere. IEEE Trans. Geosci. Electr. GE-17, 154-161.

Skolnik, M.I. (Edit.) (1970), Radar Handbook. Mc-Graw-Hill, Inc., New York.

Strauch, R.G., D.A. Merritt, K.P. Moran, K.B. Earnshaw and D. van de Kamp (1983), Tropospheric wind profiling with Doppler radar. Preprint Vol. 21th Conf. on Radar Meteor., 118-125 (publ. by Amer. Meteor. Soc., Boston, Mass.).

VanZandt, T.E. and R.A. Vincent (1983), Is VHF Fresnel reflectivity due to low frequency buoyancy waves? Preprint Vol. 21st Conf. on Radar Meteor., 126-128 (publ. by Amer. Meteor. Soc., Boston, Mass.).

VanZandt, T.E., K.S. Gage and J.M. Warnock (1981), An improved model for the calculation of profiles of C_n^2 and ε in the free atmosphere from background profiles of wind, temperature and humidity. Preprint Vol. 20th Conf. on Radar Meteor., 129-135 (publ. by Amer. Meteor. Soc., Boston, Mass.).

Vincent, R.A. and I.M. Reid (1983), HF Doppler measurements of mesospheric gravity wave momentum fluxes. J. Atmos. Sci. 40, 1321-1333.

Vincent, R.A. and J. Röttger (1980), Spaced antenna VHF radar observations of tropospheric velocities and irregularities. Radio Sci. 15, 319-335.

Vincent, R.A., W.G. Elford and B.H. Briggs (1982), A VHF radar for atmospheric studies. The Australian Physicist 19, 70-73.

Walker, J.C.G. (1979), Radar measurement of the upper atmosphere. Science 206, 180-189.

Westwater, E.R., M.T. Decker, A. Zachs and K.S. Gage (1983), Ground-based remote sensing of temperature profiles by a combination of microwave radiometry and radar. J. Climate Appl. Meteor. 22, 126-133.

Wilson, D.A. and L.J. Miller (1972), Atmospheric motion by Doppler radar. in: Remote Sensing of the Troposphere (edit. V.E. Derr), chapter 13 (Rpt. of Wave Propag. Lab., ERL, Boulder, Colorado, issued August 15, 1972).

Wilson, J., R. Carbone, H. Baynton and R. Serafin (1980), Operational application of meteorological Doppler radar. Bull. Amer. Meteor. Soc. 61, 1154-1168.

Woodman, R.F. (1981), Turbulence in the middle atmosphere: A review. Handbook for MAP, Vol. 2 (edit. S.K. Avery), 293-300 (publ. by SCOSTEP Secretariat, Univ. of Illinois, Urbana, Ill.).

Woodman, R.F. and A. Guillen (1974), Radar observations of winds and turbulence in the stratosphere and mesosphere. J. Atmos. Sci. 31, 493-505.

Woodman, R.F. and T. Hagfors (1969), Methods for the measurement of vertical ionospheric motions near the magnetic equator by incoherent scattering. J. Geophys. Res. 74, 1205-1212.

Woodman, R.F., R.P. Kugel and J. Röttger (1980), A coherent integrator-decoder preprocessor for the SOUSY-VHF-Radar. Radio Sci. 15, 233-242.

Woodman, R.F., P.K. Rastogi and T. Sato (1981), Evaluation of effective eddy diffusive coefficients using radar observations of turbulence in the stratosphere. Handbook for MAP, Vol. 2 (edit. S.K. Avery), 363-369 (publ. by SCOSTEP Secretariat, Univ. of Illinois, Urbana, Ill.).

Figure captions

Fig. 1 Range-time diagram.

Fig. 2 Altitude variation of relative reflectivity contributions for VHF radars (after Gage and Balsley, 1980).

Fig. 3 Basic principle of an MST radar system.

Fig. 4 Range-time-amplitude diagram.

Fig. 5 Time display of quadrature components in a fixed range gate.

Fig. 6 Principle of three-dimensional velocity measurements with MST VHF-radars (from Röttger, 1981b).

Fig. 7 Wind speed and direction measured with spaced antenna method (stippled distributions), aircraft (circles a) and radiosonde (circles b).

Fig. 8 Spectra measured with an elevation scan at fixed azimuth.

Fig. 9 Mean zonal (U) and meridional (V) wind velocities measured with the Arecibo radar (dots) and rawinsondes (after Fukao et al., 1982).

Fig. 10 The principle of phase measurements at antennas A_1 and A_2.

Fig. 11 Vertical velocity oscillations due to a gravity wave, measured at two slightly different zenith directions with the interferometer technique.

Fig. 12 Yagi-antennas of the SOUSY radar on Andoya/Norway, (photo:P.Czechowsky).

Fig. 13 Example of a transmitter-receiver system (after Röttger et al., 1981).

Fig. 14 Example of the digital part of an MST radar system. The functions of the parts in the dashed boxes are mostly executed by a computer (after Röttger et al., 1981).

Fig. 15 Average signal-to-noise ratio as function of altitude; the abscissa x is for $P \cdot A \cdot \Delta r = 10^7$. The abscissa x' gives log SNR for radars with given power-aperture-range gate product ($P \cdot A \cdot \Delta r$). $\tilde{S}_o$ is for $\delta_o = 0^o$, k=1.0 and A/P=0.1. $\tilde{S}_1$: $\delta_o = 0^o$, k=1.25 (z>12), k=1.2 (z<10), A/P=1. $\tilde{S}_2$: $\delta_o = 7.5^o$, $\bar{\Delta}$=0.15/deg (z=12), $\bar{\Delta}$=0.1/deg (z<10). $\tilde{S}_3$: $\delta_o = 15^o$. The circles denote measured upper heights (log SNR=0) with different radars (1,2,3=SOUSY; 4=SOUSY-Arecibo; 5=Jicamarca; 6=Pokerflat; 7=Platteville; 8=Sunset). The open circles denote vertical antenna beams, the crossed circles ⊗ denote off vertical beams ($\delta_o < 7^o$), ⊛ denote $\delta_o = 15^o$-30^o. $\sigma_{o\tilde{S}_o}$ is the log-normal standard deviation of $\tilde{S}_o$.

Fig. 16 Occurrence of MST radar echoes ($P \cdot A \sim 5 \cdot 10^7 Wm^2$) as function of season (after Balsley et al., 1983)

Fig. 17 Reflectivity contour plot (contour line difference 2 dB, the intensity of shading corresponds to the intensity of reflectivity). The bars indicate the tropopause height measured with radiosonde (from Röttger and Schmidt, 1981).

Fig. 18 Modified height-time-intensity plot showing the fine-structure of VHF-radar returns (from Hocking and Röttger, 1983).

Fig. 19 Occurrence of mesosphere echoes measured with the SOUSY-VHF-Radar at the Arecibo Observatory ($P \cdot A = 2.5 \cdot 10^8$ Wm^2).

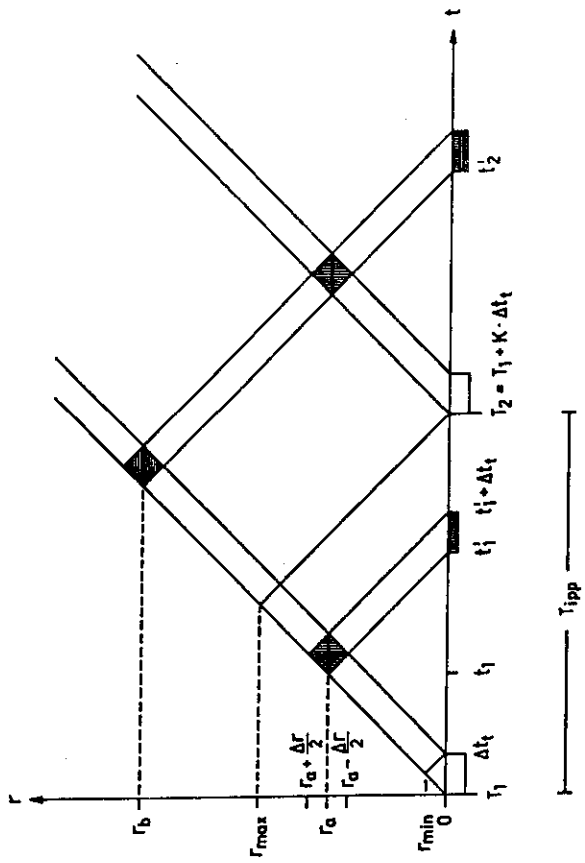

Fig 1

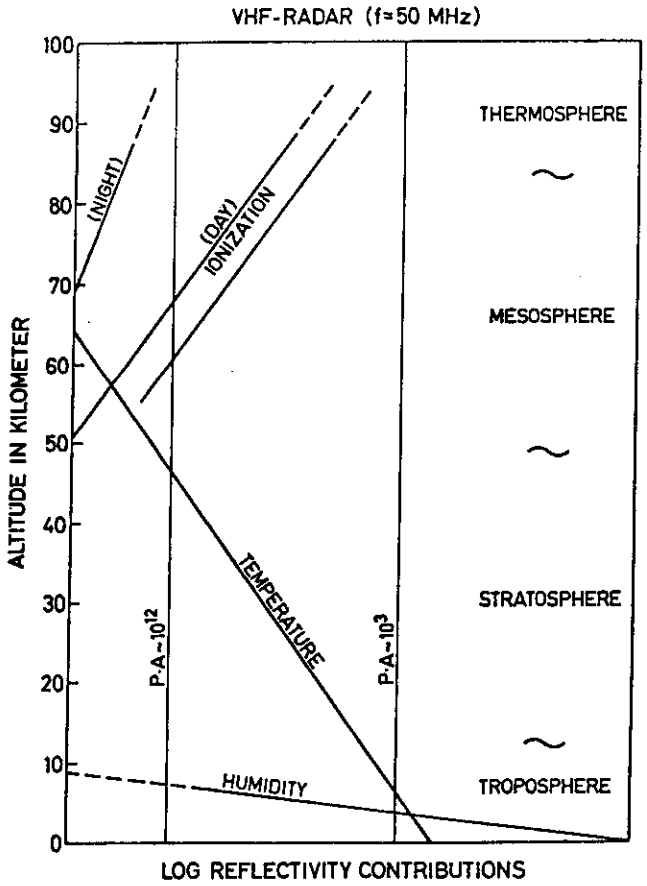
VHF-RADAR (f=50 MHz)
ALTITUDE IN KILOMETER
100
90
80
70
60
50
40
30
20
10
0
(NIGHT)
(DAY) IONIZATION
TEMPERATURE
HUMIDITY
P·A~10^12
P·A~10^3
THERMOSPHERE
MESOSPHERE
STRATOSPHERE
TROPOSPHERE
LOG REFLECTIVITY CONTRIBUTIONS

Fig 2

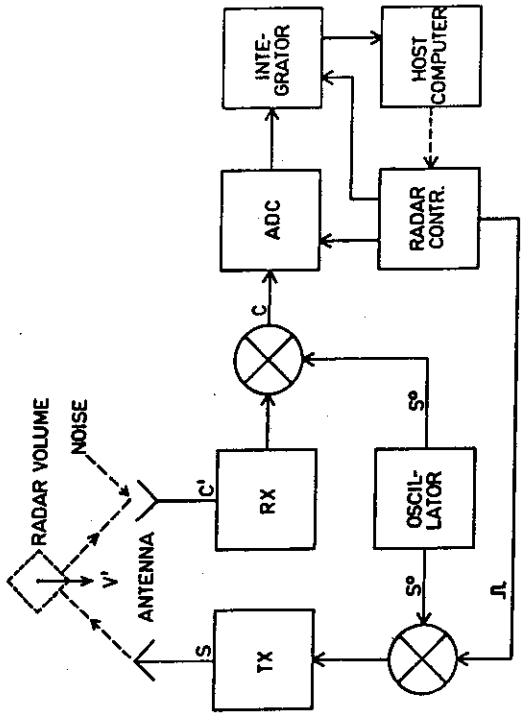
INTE-GRATOR
HOST COMPUTER
ADC
RADAR CONTR.
C
S°
RADAR VOLUME
NOISE
C'
RX
OSCIL-LATOR
V'
ANTENNA
S°
JL
S
TX

Fig 3

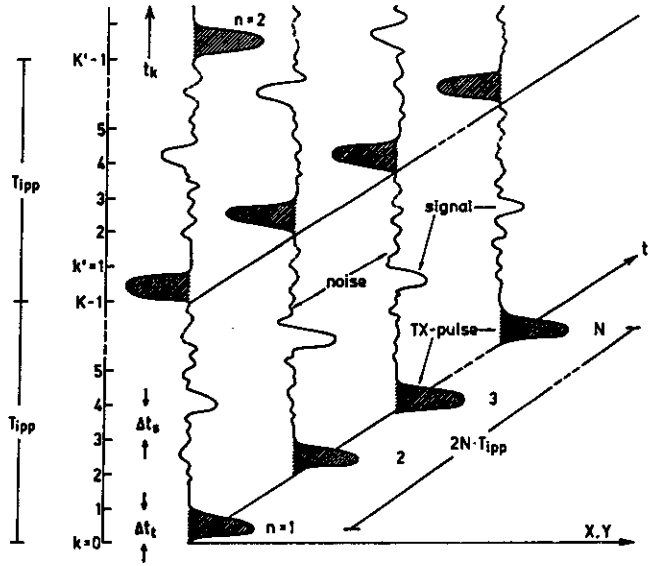
Tipp
Tipp
K'-1
5
4
3
2
k'=1
K-1
5
4
3
2
1
k=0
tk
Δts
Δtt
n=2
n=1
noise
signal
TX-pulse
t
N
3
2
2N·Tipp
X,Y

Fig 4

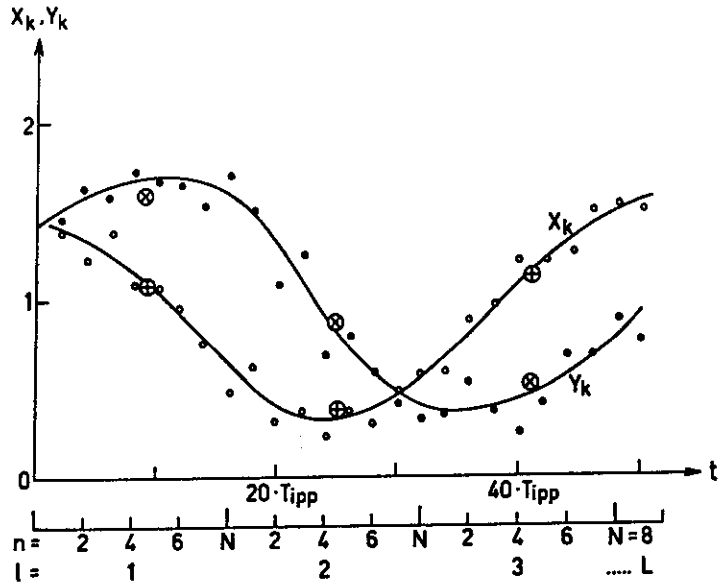
Xk,Yk
2
1
0
Xk
Yk
t
20·Tipp
40·Tipp
n= 2 4 6 N 2 4 6 N 2 4 6 N=8
l= 1 2 3 L

Fig 5

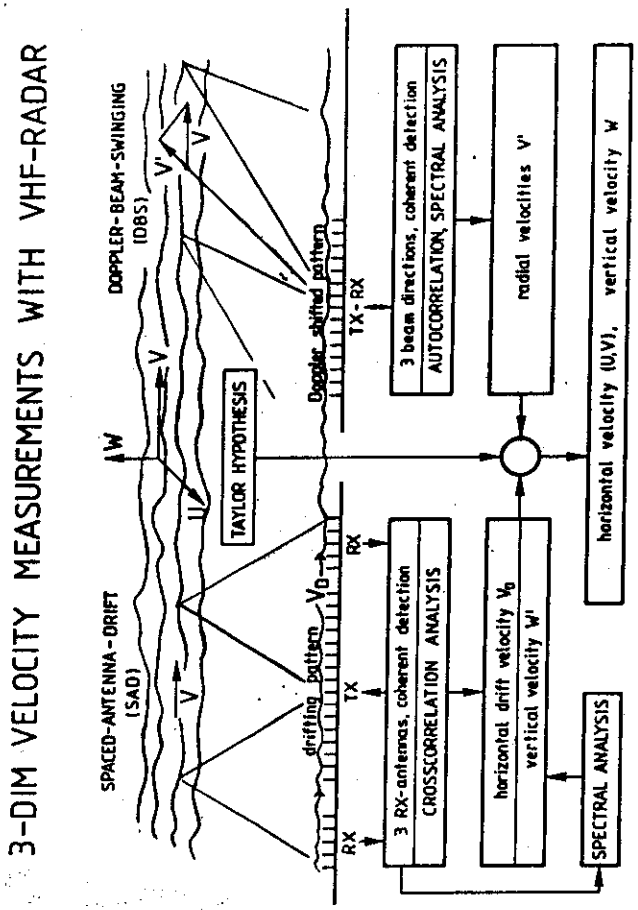
3-DIM VELOCITY MEASUREMENTS WITH VHF-RADAR
DOPPLER-BEAM-SWINGING (DBS)
SPACED-ANTENNA-DRIFT (SAD)
TAYLOR HYPOTHESIS
Doppler shifted pattern
TX-RX
drifting pattern
TX
RX
RX
3 beam directions, coherent detection
AUTOCORRELATION SPECTRAL ANALYSIS
3 RX-antennas, coherent detection
CROSSCORRELATION ANALYSIS
radial velocities V'
horizontal drift velocity V0
vertical velocity W'
SPECTRAL ANALYSIS
horizontal velocity (U,V), vertical velocity W

Fig. 6

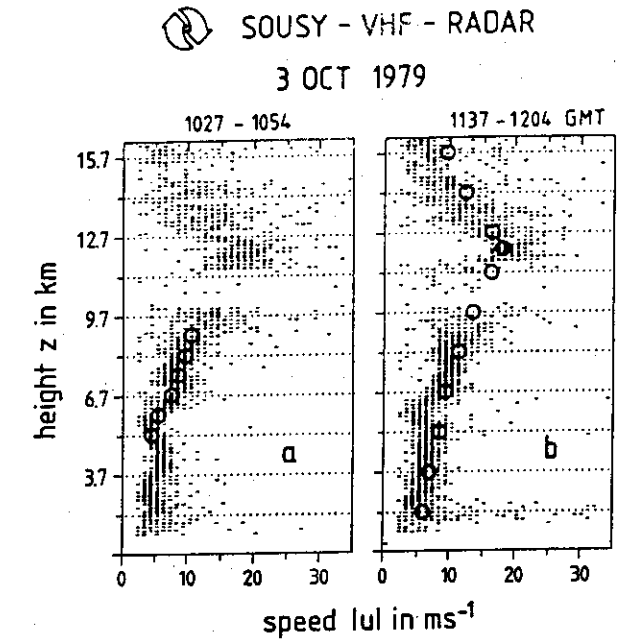
SOUSY - VHF - RADAR
3 OCT 1979
1027 - 1054
1137 - 1204 GMT
height z in km
15.7
12.7
9.7
6.7
3.7
a
b
0
10
20
30
speed |u| in ms-1

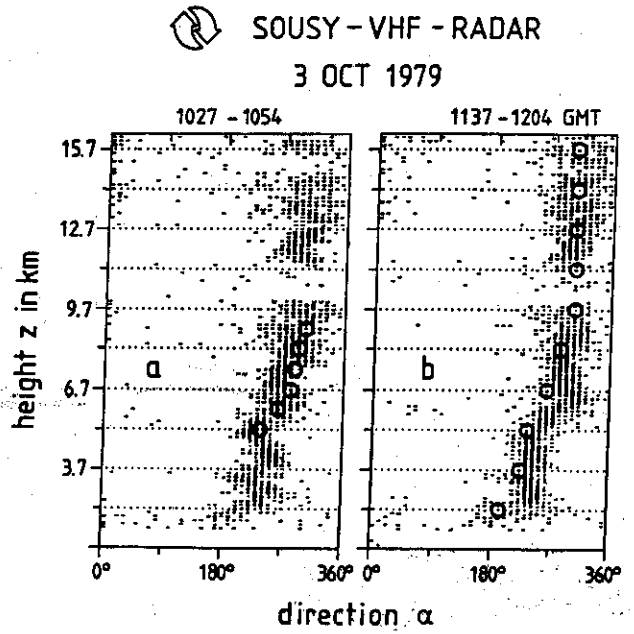
SOUSY - VHF - RADAR
3 OCT 1979
1027 - 1054
1137 - 1204 GMT
height z in km
15.7
12.7
9.7
6.7
3.7
a
b
0°
180°
360°
direction α

Fig. 7

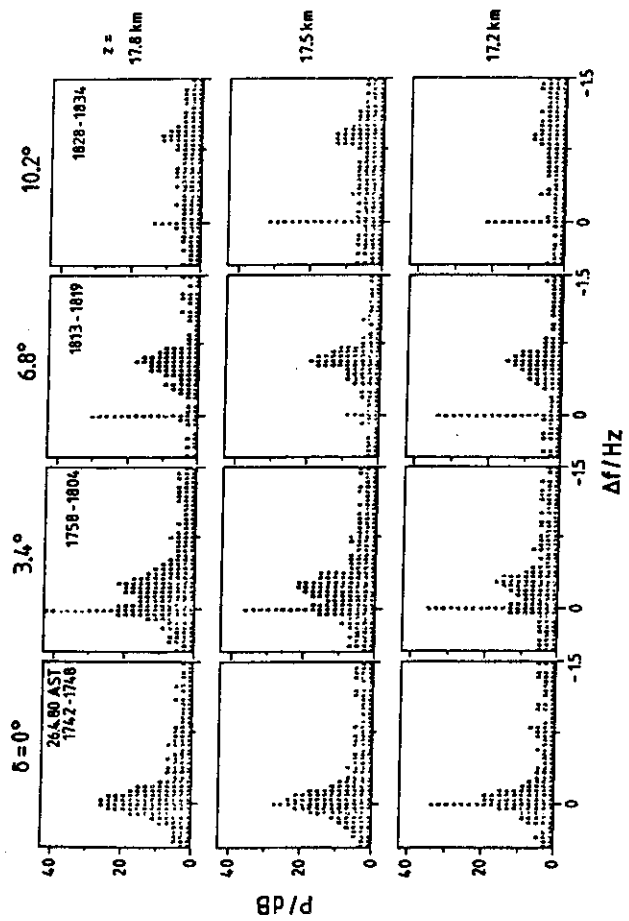
z = 17.8 km
17.5 km
17.2 km
10.2°
6.8°
3.4°
δ=0°
1828-1834
1813-1819
1758-1804
26.4.80 AST
1742-1748
-15
0
Δf/Hz
40
20
0
dB/d

Fig 8

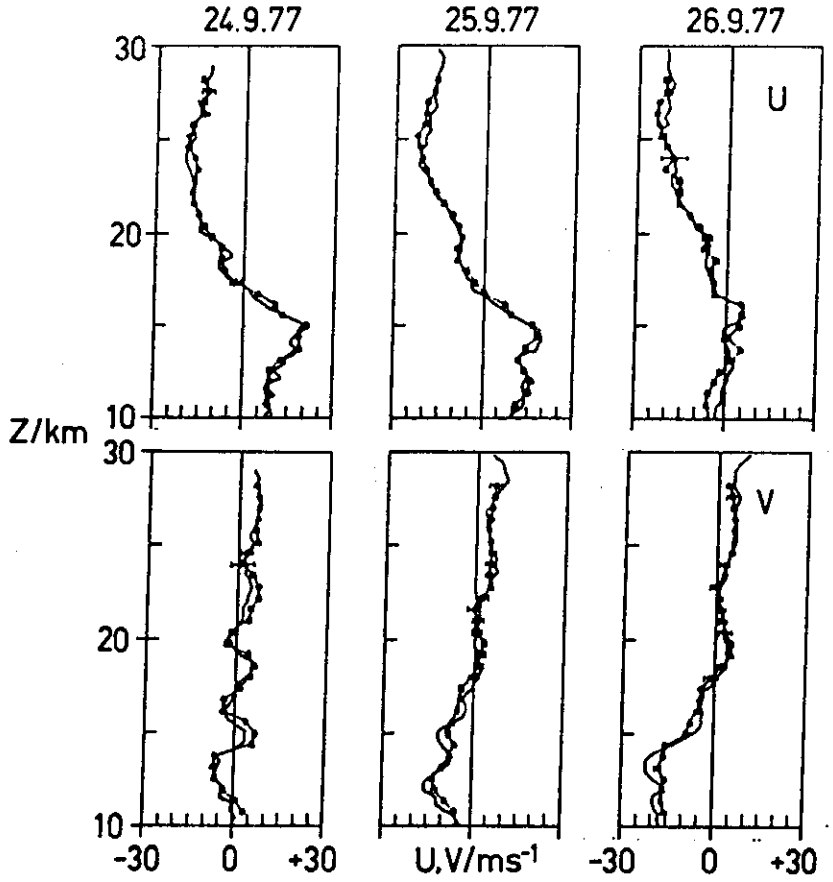
24.9.77
25.9.77
26.9.77
U
V
Z/km
30
20
10
-30
0
+30
U,V/ms⁻¹

Fig 9

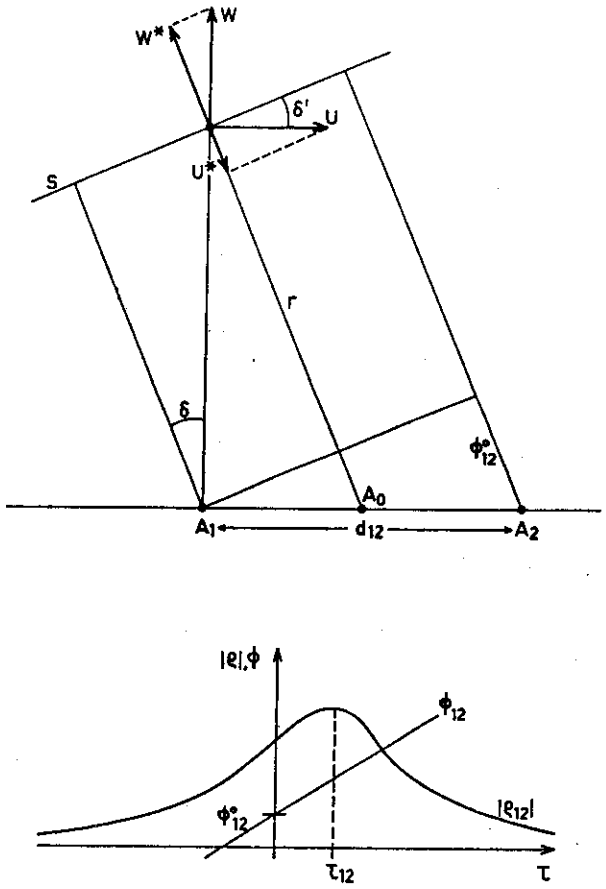
w*
w
δ'
U
U*
s
r
δ
ϕ^o_{12}
A_0
A_1
d_{12}
A_2
|ϱ|,ϕ
ϕ_{12}
ϕ^o_{12}
$|\varrho_{12}|$
τ_{12}
τ

Fig 10

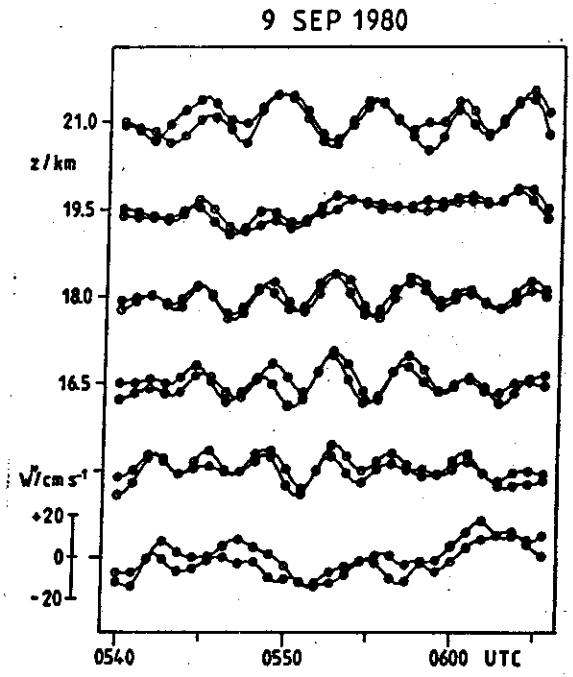
9 SEP 1980
21.0
z/km
19.5
18.0
16.5
w/cm s⁻¹
+20
0
-20
0540
0550
0600 UTC

Fig 11

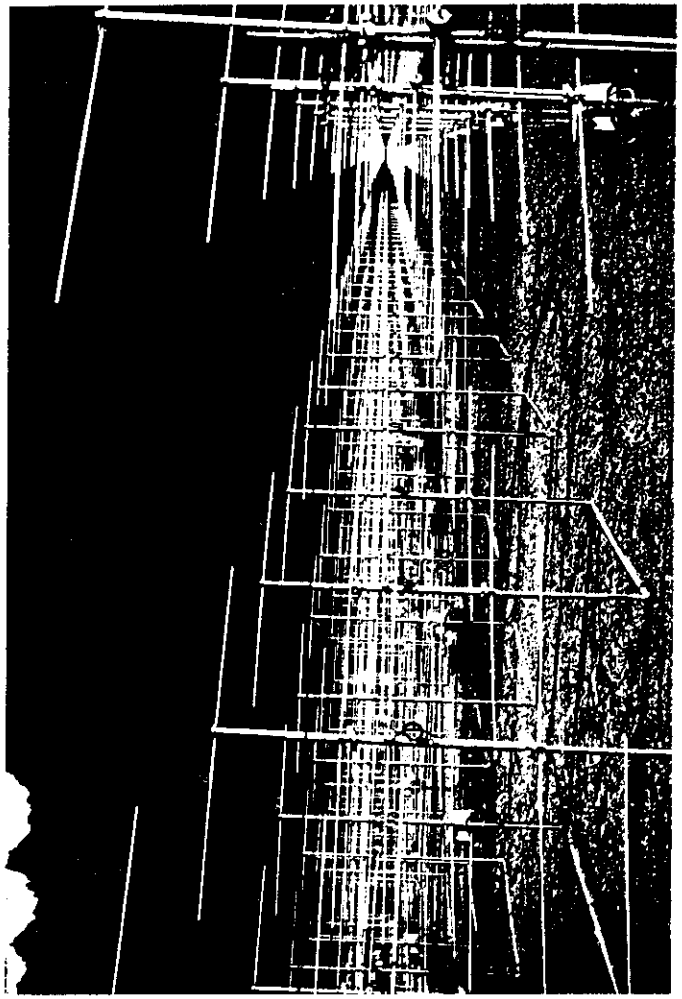

Fig 12

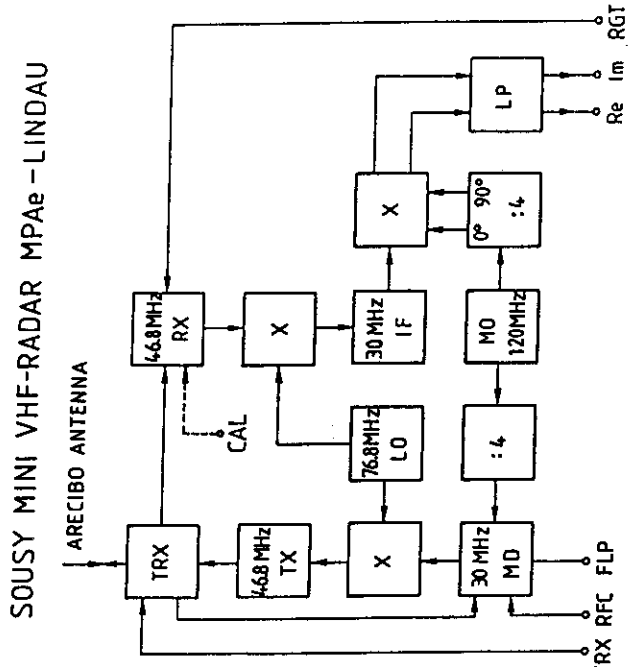
SOUSY MINI VHF-RADAR MPAe-LINDAU
ARECIBO ANTENNA
TRX
TRX RFL FLP
468 MHz TX
468 MHz RX
CAL
X
76.8 MHz LO
X
30 MHz IF
X
30 MHz MD
:4
MO 120 MHz
0° 90°
:4
LP
Re Im RGT

Fig 13

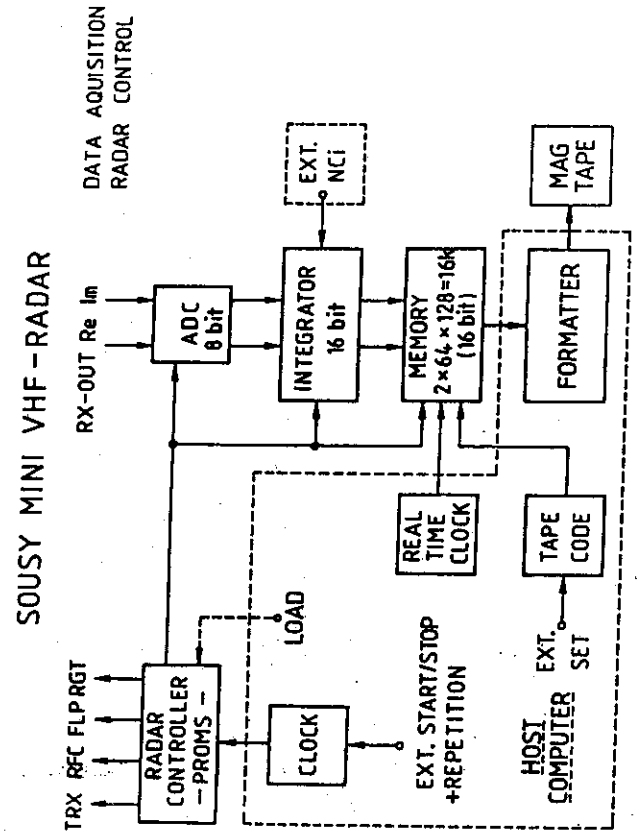
SOUSY MINI VHF-RADAR
DATA AQUISITION
RADAR CONTROL
RX-OUT Re Im
TRX RFC FLP RGT
ADC
8 bit
INTEGRATOR
16 bit
EXT.
NCI
MEMORY
2×64×128=16K
(16 bit)
FORMATTER
MAG
TAPE
RADAR
CONTROLLER
-PROMS-
CLOCK
LOAD
EXT. START/STOP
+REPETITION
REAL
TIME
CLOCK
TAPE
CODE
EXT.
SET
HOST
COMPUTER

Fig 14

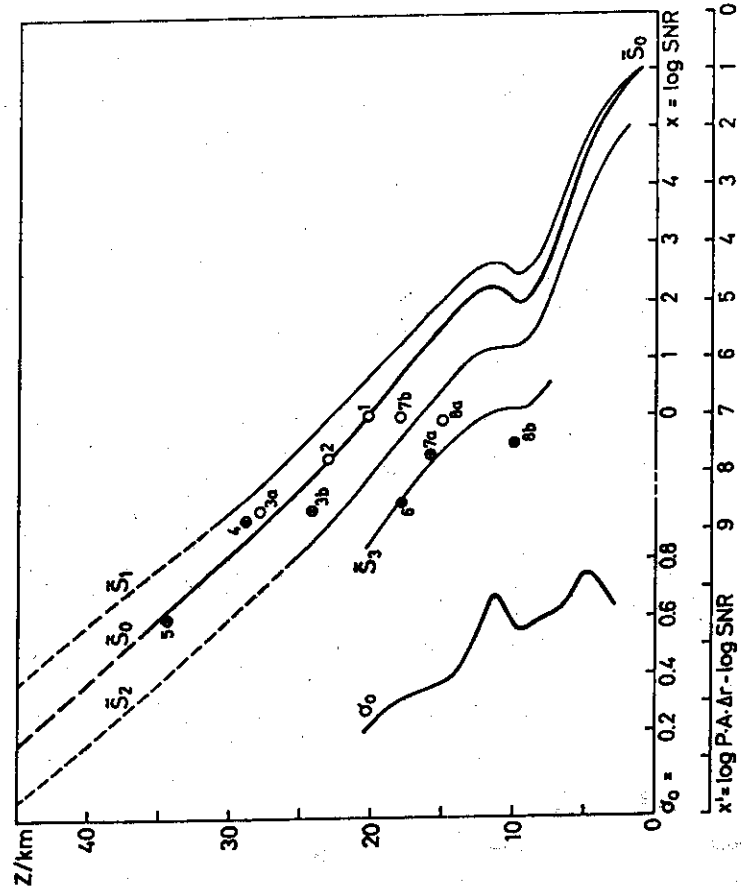
Z/km
40
30
20
10
0
$\bar{S}_1$
$\bar{S}_0$
$\bar{S}_2$
$\bar{S}_3$
$\bar{S}_0$
σ_0
σ_0 = 0 0.2 0.4 0.6 0.8
x = log SNR
$x' = \log P \cdot A \cdot \Delta r - \log SNR$
0 1 2 3 4 5 6 7 8 9

Fig 15

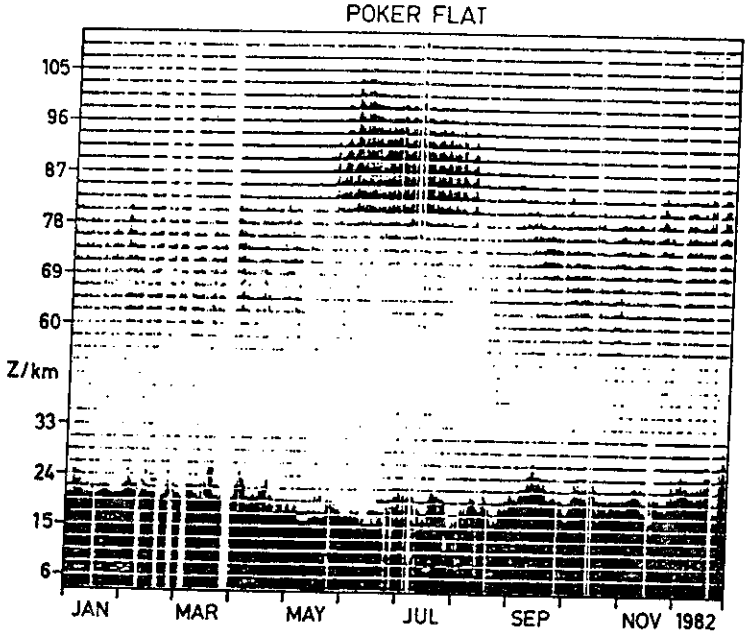
POKER FLAT
105
96
87
78
69
60
Z/km
33
24
15
6
JAN
MAR
MAY
JUL
SEP
NOV 1982

Fig 16

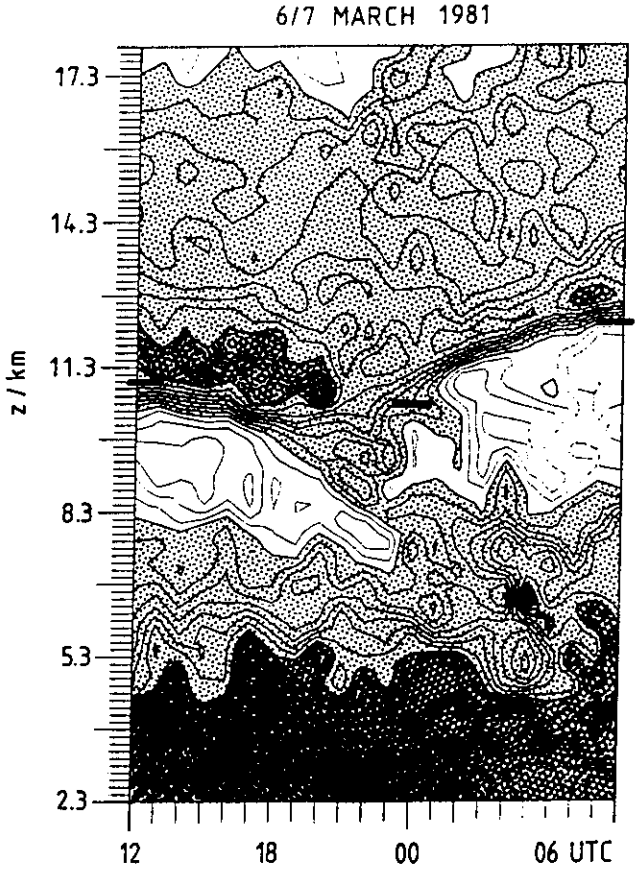
6/7 MARCH 1981
17.3
14.3
11.3
8.3
5.3
2.3
z / km
12
18
00
06 UTC

Fig 17

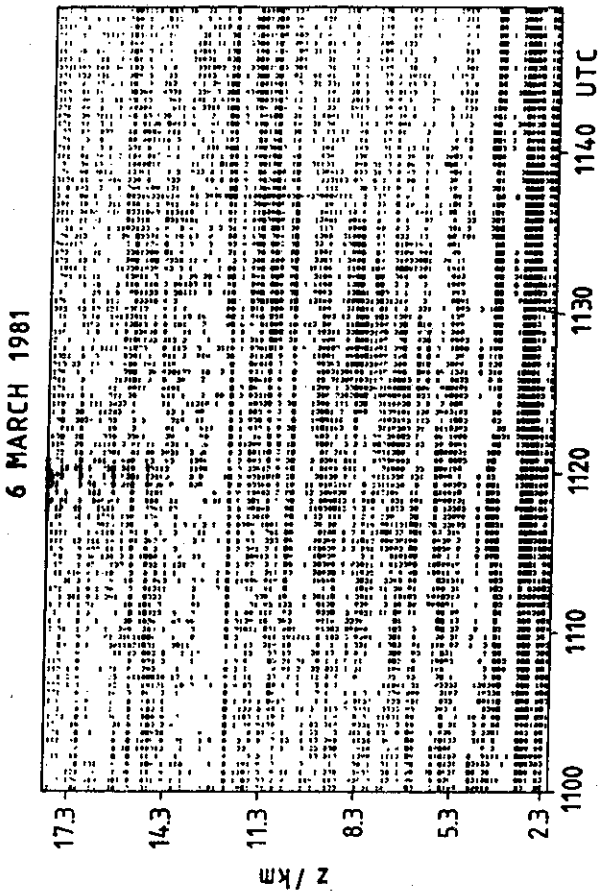
6 MARCH 1981
z / km
17.3
14.3
11.3
8.3
5.3
2.3
1100
1110
1120
1130
1140 UTC

Fig. 18

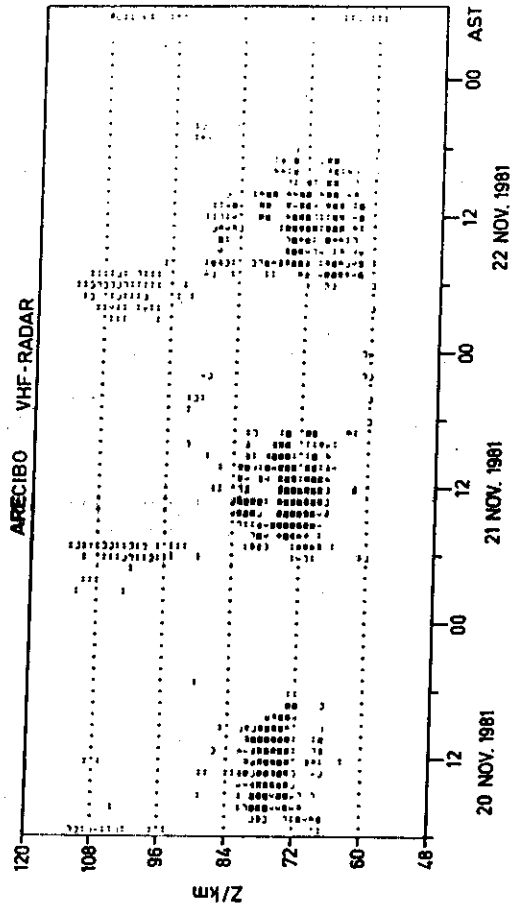
ARECIBO VHF-RADAR
Z/km
120
108
96
84
72
60
48
20 NOV. 1981
12
00
21 NOV. 1981
12
00
22 NOV. 1981
12
00 AST

Fig 19

Table I OPERATIONAL AND PLANNED MST/ST/IS RADARS (NOVEMBER 1983)

facility	mode	lat./long. deg.	freq. MHz	ave.power kW	min.pulse width μs	duty cycle (max.)%	antenna aperture (eff.)m²	antenna beam width	antenna configuration	antenna mode	steerability	status	ref.
Arecibo/Puerto Rico	IS, ST	19N,67W	430	120	1	6	50000	0.17°	circ.dish	DB	20°(m)	op	(1)
" / "	MST		46.8	1	1	2	50000	1.7°	"	DB	"	cs	
Buckland Park/Australia	(M)ST	35S,138E	54.1	0.4	7	0.7	7500	3.2°	PAC,PAY	DB,SA	15°(1)	(op)	(2)
Chung-Li/Taiwan	(M)ST	25N,121E	52	4	1	2	2500	5°	PAY	DB,SA	15°(2)	cs	(3)
EISCAT/	IS,ST	70N (67N)	933.5	250	2	12.5	520	0.6°	3 circ.dishes	DB	60°(m),tristat.	op	(4a)
North Scandinavia	IS,ST	19E (27E)	224	600	2	12.5	3300	0.6°,1.7°	cyl.dish	DB	30°,60°,20°(m)	cs	(4b)
Equatorial Pacific	ST (3x)	(0,150E)	49.8	0.2	5	(2)	(5000)	(5°)	PAC	DB	15°(2)	pl/cs	(5)
India	MST	—	45-55	60	1	2.5	20000	3°	PAC	DB	20°(2)	pl	(6)
Jicamarca/Peru	MST,IS	12S,72W	49.9	200	(1)	5	80000	1.06	PAC	DB,SA	3°(m)	op	(7)
LSEET/France	ST	43N,5E	47.8	1	2	1.7	3x2000	5°	PAC	DB	15°(2)	cs	(8)
Millstone Hill/USA	IS,ST	43N,72W	440	30	2	1.6	1640	1°	circ.dish	DB	<80°(m)	op	(9)
MU/Japan	MST,(IS)	35N,136E	46.5	50	1	5	8330	3.6°	PAY	DB,SA	30°(m)	(op)	(10)
Penn.State/USA	ST (3x)	41N,78W	48-50	1	4	2	2500	5°	PAC	DB	15°(2)	pl	(11)
Platteville/USA	ST (4x)	40N,105W	49.8	1	4	1.7	2000	5°	PAC	DB	15°(2)	op/rt	(12)
Poker Flat/USA	MST	65N,147W	49.9	128	2	2	40000	1.4°	PAC	DB	15°(2)	op/rt	(13)
PROUST/France	ST	45N,2E	935	(~10)	4 (0.2)		2000 (95)		2 dishes	DB	bistatic	(pl)	(14)
Sondre Stromfjord/Greenland	IS,ST	67N,51W	1290	100	(1)	3	420	0.5°	circ.dish	DB	90°(m)	op	(15)
SOUSY/Germany	MST	52N,10E	53.5	24	1	4	3200	5°	PAY	DB,SA	12.5°(m)	op	(16a)
" /Norway	MST	69N,16E	53.5	8	1	4	8800	3°	PAY	DB	4.0°(2),5.6°	op	(16b)
Sunset/USA	ST	40N,106W	40.5	16	1	2.5 (16)	2200	4.4°,4.8°	PAC	DB	60°(2,m)	op	(17)
United Kingdom	MST	—	~50	12	1	5	5200	3.6°	PAY	DB	5°,10°(2)	pl	(18)
Urbana/USA	MST	40N,88W	40.9	6	10	1	2000	(<3°)	PAD	DB	1.5°(1),2.5°(2)	op	(19)

mode: IS = incoherent scatter (thermosphere, may include mesosphere)
MST = mesosphere,stratosphere,troposphere
ST = stratosphere,troposphere

antenna:
configuration: PA = phased array
PAC = phased array, coaxial-collinear dipoles
PAD = phased array, dipoles
PAY = phased array, Yagis

mode: DB = Doppler beam swinging
SA = spaced antenna (interferometer)

steerability: 15°(2) = zenith angle 15° in 2 orthogonal planes (and zenith)
15°(m) = multiple position out to 15° zenith angle (and zenith)

status: op = operational
op/rt = routine operation (continuous)
cs = under construction
pl = planned

ref.: (1) Woodman+); (2) Vincent et al., 1982; (3) Brosnahan et al.+); (4a) Röttger et al.+); (4b) Hagfors et al., 1982; (5) Balsley+); (6) Koshy+); (7) Woodman and Guillén, 1974, Woodman and Ferlay+); (8) Crochet+); (9) Rastogi+); (10) Kato+); (11) Peters+); (12) Strauch et al., 1983, Strauch+); (13) Balsley et al., 1980, Balsley et al.+); (14) Glass+); (15) Watkins+); (16a) Röttger et al., 1978; (16b) Czechowsky et al.+); (17) Green et al., 1975, Green+); (18) Hall+); (19) Røyrvik and Goss+)

+) = in: Bowhill (1984), Handbook for MAP 9.